Electronics and Electrical Engineering

https://www.aimspress.com/journal/ElectrEng

AIMS Electronics and Electrical Engineering, 10(2): 285–313.
DOI: 10.3934/electreng.2026012
Received: 03 February 2026
Revised: 27 February 2026
Accepted: 06 March 2026
Published: 03 April 2026

Research article

Fixed-time filtered backstepping control for quadrotor UAVs with an adaptive fixed-time disturbance observer

Mohammed Rida Mokhtari[1,2,*], Abdelkader Ghezouani[1], Bensalah Choukri[2], Amal Choukchou Braham[2] and Hicham Megnafi[1]

[1] École supérieure en sciences appliquées de Tlemcen, Algeria

[2] Laboratoire d'Automatique de Tlemcen (LAT). Electrical Engineering Department, Tlemcen University, Algeria

* **Correspondence:** Email: rida.mokhtari@essa-tlemcen.dz.

Abstract: This work has proposed a novel robust fixed-time tracking control scheme for quadrotor unmanned aerial vehicles subject to unknown external disturbances and model uncertainties. Accounting for the inherent underactuated dynamics of the quadrotor, a hierarchical control architecture was constructed that decouples position and attitude regulation into two separate control loops, namely, an outer loop dedicated to translational motion and an inner loop responsible for rotational dynamics. The proposed framework integrates a fixed-time backstepping design with a command filtering technique to mitigate the explosion-of-complexity problem that typically arises in conventional backstepping approaches, while simultaneously guaranteeing fixed-time convergence of the tracking errors. To effectively address the effects of model uncertainties and external perturbations acting on the system, an adaptive fixed-time disturbance observer was introduced and integrated into the control architecture. This observer is capable of accurately estimating the unknown disturbances and uncertainties, achieving estimation convergence within a predetermined time that remains independent of the initial conditions of the system. Rigorous stability analysis based on Lyapunov theory was carried out to establish the fixed-time convergence of the tracking errors to a bounded neighborhood of the origin. Comprehensive numerical simulations were performed on a quadrotor system, and the results obtained were compared against several existing control methods. The comparative analysis clearly demonstrated that the proposed controller achieves superior tracking accuracy, faster convergence, and improved disturbance rejection performance compared to the alternate approaches considered.

Keywords: quadrotor; UAV; backstepping; cascade architecture; fixed time; disturbance observer; adaptive observer; nonlinear filter

1. Introduction

A substantial body of research has been dedicated to advancing a diverse range of robotic platforms, encompassing unmanned aerial vehicles (UAVs) [1], autonomous vehicles [2], underwater vehicles [3], robot manipulators [4], and aerial manipulators [5]. Among these, multirotor unmanned aerial vehicles (MUAVs) have emerged as particularly compelling platforms, owing to their distinctive operational capabilities, including vertical takeoff and landing, precise hovering, and agile low-velocity flight. Such characteristics render MUAVs exceptionally well-suited for deployment in confined or GPS-denied environments, as well as in areas devoid of conventional infrastructure. In contrast to fixed-wing UAVs, which inherently rely on runways or dedicated launching mechanisms, multirotor systems are capable of autonomously navigating to designated target locations while sustaining stable flight over extended operational periods. The quadrotor configuration has become particularly prevalent due to its simple mechanical design, fourfold rotational symmetry, and excellent maneuverability characteristics. By utilizing four motors mounted in a planar arrangement, quadrotors achieve attitude regulation through differential variations in rotor speeds, resulting in a compact architecture with inherent actuator redundancy. The key advantages of this design include well-balanced aerodynamic properties, favorable power-to-weight ratios, and resilience to environmental disturbances.

The control of multirotor aerial vehicles has been extensively investigated through numerous robust and adaptive methodologies in the recent literature. Robust control strategies constitute a major research direction. For instance, [6] combined approximate linearization control with disturbance observers. A geometric framework for disturbance compensation in gun-launched quadrotors was developed in [7]. In [8], extended state observers were integrated with a sliding mode control to improve trajectory tracking under environmental disturbances. Adaptive control techniques have also proven effective for such platforms. Neural network-based adaptive schemes for small UAV tracking were investigated in [9]. Fuzzy adaptive integral backstepping with command filtering was employed to handle input-constrained quadrotor control in [10]. In [11], the authors reviewed fractional-order control laws for manipulators, mobile robots, human–robot systems, and bio-inspired robots, emphasizing control design, fractional calculus definitions, performance enhancement, and controller tuning methods. The immersion and invariance principle was employed to enable adaptive trajectory tracking for coaxial tilt-rotor vehicles in [12]. A fault-tolerant control strategy combining adaptive backstepping with radial basis function (RBF) neural networks for aerial manipulators was presented in [13]. An intelligent control architecture combining artificial neural networks (ANNs) and proportional–integral–derivative (PID) control was developed in [14], where the neural network continuously updates the PID gains to enhance online adaptability. In [15], the authors proposed a fractional neural integral sliding-mode controller for a robot manipulator on a free-floating satellite, based on the Caputo-Fabrizio derivative and Riemann–Liouville integral.

Finite-time and fixed-time control approaches have gained prominence for guaranteeing rapid and predictable convergence in aerial robotics. Disturbance observers coupled with nonsingular terminal sliding modes were proposed to provide fixed-time formation control for autonomous underwater vehicles (AUVs) in [16]. Incremental backstepping with fixed-time convergence was employed to improve damaged aircraft flight control in [17]. Constrained finite-time attitude control for fixed-wing UAVs under actuator saturation was addressed in [18]. Event-triggered adaptive barrier function-based sliding modes were utilized to ensure fixed-time fault-tolerant quadrotor control in [19]. A safety-

constrained finite-time vector field control strategy for quadrotor trajectory tracking was presented in [20]. A fixed-time carrier landing control scheme under external disturbances was developed in [21].

Many prior studies have addressed finite-time and fixed-time control, disturbance observation, and hierarchical flight architectures. However, most of these approaches have notable limitations. Some rely on restrictive assumptions regarding disturbance characteristics, while others employ a dynamic extension of the thrust control input, leading to more complex control equations. Additionally, flatness-based controllers are often unable to estimate disturbances acting on the planar axes (i.e., roll and pitch dynamics), and classical disturbance observers typically assume that disturbances are bounded by a known constant, which limits their practical applicability.

In light of these research gaps, this work proposes an original fixed-time robust control (FxTRC) framework for quadrotor trajectory tracking, integrating hierarchical filtered fixed-time backstepping with an adaptive fixed-time disturbance estimation scheme. The proposed approach advances the UAV research field by offering a unified and rigorously validated control architecture that simultaneously ensures fixed-time convergence, robustness against uncertainties and external disturbances, and practical implementability for complex underactuated aerial systems. The first key contribution lies in the integration of a fixed-time command-filtered controller within a hierarchical flight control framework, in which the overall control problem is systematically decomposed into two interconnected layers: an outer-loop position controller and an inner-loop attitude controller. This hierarchical decomposition effectively decouples the translational and rotational dynamics, facilitating a structured control design, a tractable stability analysis, and enhanced real-time implementability, while ensuring globally stable flight performance. Moreover, by embedding a command-filtering mechanism into the recursive backstepping procedure, the proposed controller guarantees fixed-time stability with settling-time bounds that are explicitly independent of initial conditions, while avoiding the explosion-of-complexity issue inherent to conventional backstepping formulations. This integration yields smoother control signals, reduces computational overhead, and strengthens real-time feasibility, all while preserving rigorous theoretical stability and convergence guarantees. The second contribution is the design of an adaptive disturbance observer with provable fixed-time convergence properties, seamlessly incorporated into the proposed control framework. The adaptive mechanism continuously updates its internal parameters in response to instantaneous estimation errors, without requiring any prior knowledge of the magnitude, structure, or frequency content of the disturbances. This online adaptation enables accurate real-time tracking and reconstruction of time-varying external disturbances and lumped uncertainties, effectively compensating for their adverse effects on the closed-loop dynamics. The adaptive parameters in the proposed observer are derived by extending the adaptive laws introduced in [23], where the convergence conditions are reformulated to be fully consistent with the fixed-time stability framework of the proposed controller. Consequently, the observer achieves precise disturbance estimation within a guaranteed fixed-time bound, even under highly uncertain and rapidly varying perturbations. Furthermore, the observer operates concurrently across both the translational and rotational subsystems, enabling active compensation of lumped uncertainties and external perturbations, which substantially enhances disturbance rejection, reinforces closed-loop robustness, and preserves high steady-state tracking accuracy under challenging operating conditions.

This paper is organized as follows. Section 2 describes the quadrotor system dynamics. The fixed-time controller synthesis and the corresponding stability proofs are presented in Section 3. Section 4 demonstrates the proposed approach through numerical simulations and comparative analysis. Finally,

Section 5 presents the concluding remarks.

2. System description and preliminaries

2.1. System description

This section presents the mathematical model of the quadrotor UAV dynamics. The coordinate frames and the UAV components are shown in Figure 1. The quadrotor consists of a rigid central body equipped with four brushless DC motor-driven rotors, symmetrically arranged to generate the lift and control moments required for both translational and rotational motion. We define $\mathcal{B} := (O_b, x_b, y_b, z_b)$ as the body-fixed reference frame attached to the vehicle at its center of mass, while $\mathcal{I} := (O_e, x_e, y_e, z_e)$ designates the inertial reference frame. The position of the center of mass expressed in $\mathcal{I}$ is given by $\xi = (x, y, z)^T$. The attitude is characterized by $\eta = (\phi, \theta, \psi)^T$, representing roll ($\phi$), pitch ($\theta$), and yaw ($\psi$) angles, with the constraints $-\frac{\pi}{2} < \phi < \frac{\pi}{2}$, $-\frac{\pi}{2} < \theta < \frac{\pi}{2}$, and $-\pi < \psi < \pi$. The rotation matrix $\mathcal{R}_\eta$ that maps vectors from $\mathcal{B}$ to $\mathcal{I}$ is given as:

$$\mathcal{R}_\eta = \begin{bmatrix} \cos\psi\cos\theta & \cos\psi\sin\theta\sin\phi - \sin\psi\cos\phi & \cos\psi\sin\theta\cos\phi + \sin\psi\sin\phi \\ \sin\psi\cos\theta & \sin\psi\sin\theta\sin\phi + \cos\psi\cos\phi & \sin\psi\sin\theta\cos\phi - \cos\psi\sin\phi \\ -\sin\theta & \cos\theta\sin\phi & \cos\theta\cos\phi \end{bmatrix} \tag{2.1}$$

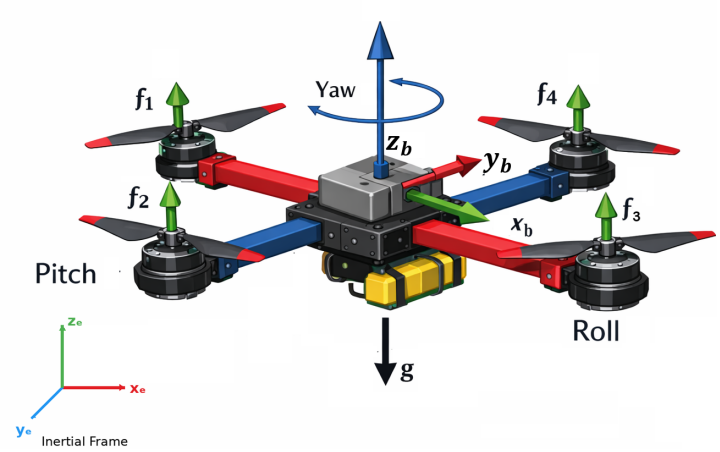

Figure 1. Coordinate frames and dynamic configuration of the quadrotor UAV.

The translational dynamics of the quadrotor UAV are described by

$$m\ddot{\xi} = \mathbf{T}^b \mathcal{R}_\eta z_e - mgz_e + \bar{d}_{ext} \tag{2.2}$$

where $m \in \mathbb{R}$ denotes the total vehicle mass, g represents the gravitational acceleration constant, and $\bar{d}_{ext} = [\bar{d}_x, \bar{d}_y, \bar{d}_z]^T$ denotes the external disturbance vector. The combined thrust force $\mathbf{T}^b = [0, 0, T_z]^T$ acts along the body-fixed z-axis, with z_e denoting the unit vector along the z-axis of the inertial frame. The total thrust T_z is defined as

$$T_z = \sum_{i=1}^{4} \varrho_i \Omega_i^2 \tag{2.3}$$

where $\varrho_i > 0$, $i \in \{1, 2, 3, 4\}$, are the thrust coefficients, and Ω_i denotes the angular speed of the i-th rotor.

The angular motion of the aerial vehicle is described using the Newton–Euler formalism

$$\mathbb{J}(\eta)\ddot{\eta} + C(\eta, \dot{\eta})\dot{\eta} = \tau + \bar{\tau}_{ext} \tag{2.4}$$

Here, the generalized inertia matrix is defined as $\mathbb{J}(\eta) = \Xi^T J \Xi$, which is positive definite. The external disturbances are represented by $\bar{\tau}_{ext} = [\bar{d}_\phi, \bar{d}_\theta, \bar{d}_\psi]^T$, and the applied control torques $\tau = [\tau_\phi, \tau_\theta, \tau_\psi]^T$ are given by

$$\tau = \begin{bmatrix} -l\varrho(\Omega_2^2 - \Omega_4^2) \\ -l\varrho(\Omega_1^2 - \Omega_3^2) \\ \bar{\varrho}(\Omega_1^2 - \Omega_2^2 + \Omega_3^2 - \Omega_4^2) \end{bmatrix} \tag{2.5}$$

Here, l denotes the distance between each rotor center and the vehicle center of gravity, and $\bar{\varrho} > 0$ is a positive constant characterizing the aerodynamic properties of the propellers.

From (2.2) and (2.4), the quadrotor dynamics can be reformulated as follows

$$\begin{cases} \dot{\xi} = \upsilon, \\ \dot{\upsilon} = \frac{T_z}{m}\mathcal{R}_\eta z_e - g z_e + d_{ext} \\ \dot{\eta} = \omega \\ \dot{\omega} = \tau - C(\eta, \dot{\eta})\,\dot{\eta} + \tau_{ext} \end{cases} \tag{2.6}$$

where the vectors υ and ω correspond to the translational and angular velocities in $\mathcal{I}$, respectively, while the normalized external disturbances are defined as

$$d_{ext} = \frac{1}{m}\bar{d}_{ext}, \quad \tau_{ext} = \mathbb{J}^{-1}\bar{\tau}_{ext}$$

2.2. Preliminaries

Essential preliminaries concerning fixed-time stability theory and related useful inequalities are presented below, which serve as the theoretical foundation for the fixed-time (FxT) controller's stability analysis.

Definition 1. *Consider a dynamical system described by:*

$$\dot{x} = f(x), \quad f(0) = 0, \quad x \in \Phi \subset \mathbb{R}^n \tag{2.7}$$

where $f : \Phi \times \mathbb{R}^+ \to \mathbb{R}^n$ represents a continuous function mapping from an open set Φ containing the equilibrium point $x = 0$ and the nonnegative reals into $\mathbb{R}^n$.

Lemma 1. *[22] Consider system (2.7) with a Lyapunov function $V(x)$ and positive scalars a, b, m, and n, where $0 < m < 1$ and $n > 1$. If the following inequality holds:*

$$\dot{V}(x) \leq -(aV(x)^m + bV(x)^n) + \vartheta_0 \tag{2.8}$$

with $\vartheta_0 > 0$, then the system achieves practical fixed-time stability. The ultimate bound of the state trajectories is given by

$$\lim_{t\to T_r} V(x(t)) \le \min\left\{a^{-\frac{1}{m}}\left(\frac{\vartheta_0}{1-\varrho_0}\right)^{\frac{1}{m}},\ b^{-\frac{1}{n}}\left(\frac{\vartheta_0}{1-\varrho_0}\right)^{\frac{1}{n}}\right\} \tag{2.9}$$

with $0 < \varrho_0 < 1$. Additionally, the convergence time satisfies

$$T_r \le \frac{1}{a\varrho_0(1-m)} + \frac{1}{b\varrho_0(n-1)} \tag{2.10}$$

Lemma 2. *[23] For $\mathbf{z_1}, \mathbf{z_2} \in \mathbb{R}$, and $\varphi_1 > 0$, $\varphi_2 > 0$, the following inequality holds:*

$$|z_1|^{\varphi_1}|z_2|^{\varphi_2} \le \frac{\varphi_1}{\varphi_1+\varphi_2}\phi|z_1|^{\varphi_1+\varphi_2} + \frac{\varphi_2}{\varphi_1+\varphi_2}\phi^{-\frac{\varphi_1}{\varphi_2}}|z_2|^{\varphi_1+\varphi_2}, \quad \phi > 0 \tag{2.11}$$

Lemma 3. *[24] For $z_1 \le z_2$ and $\varphi_0 > 1$, the following inequality holds:*

$$z_1(z_2-z_1)^{\varphi_0} \le \frac{\varphi_0}{\varphi_0+1}(z_2^{\varphi_0+1} - z_1^{\varphi_0+1}) \tag{2.12}$$

Lemma 4. *[25] For $i \in \{1, 2, \ldots, n\}$, $0 < p_0 \le 1$, and $q_0 > 1$, the following inequalities hold:*

$$\Big(\sum_{i=1}^{n}|z_i|\Big)^{p_0} \le \sum_{i=1}^{n}|z_i|^{p_0} \tag{2.13}$$

$$n^{1-q_0}\Big(\sum_{i=1}^{n}|z_i|\Big)^{q_0} \le \sum_{i=1}^{n}|z_i|^{q_0} \tag{2.14}$$

Lemma 5. *[26] For $\{\bar{a}, \bar{b}, \bar{c}\} > 0$ and positive real constants p and q satisfying $\frac{1}{p} + \frac{1}{q} = 1$, the following inequality holds:*

$$\bar{a}\bar{b} \le \bar{c}^{p}\frac{\bar{a}^{p}}{p} + \bar{c}^{-q}\frac{\bar{b}^{q}}{q} \tag{2.15}$$

3. Controller design and stability analysis

This section develops a trajectory-tracking controller for the quadrotor system that explicitly accounts for unknown external disturbances and uncertainties. The proposed control architecture consists of two main components. First, cascaded fixed-time backstepping is employed to design the control laws: the inner loop generates control moments for attitude regulation, while the outer loop produces thrust commands for position control. To avoid the explosion of complexity typically encountered in classical backstepping designs, a fixed-time command filter is introduced to provide smooth estimates of the virtual control signals and their derivatives. Second, a novel adaptive fixed-time disturbance observer (AFxTDO) is proposed to estimate the lumped system disturbances within a guaranteed fixed-time bound. The integration of the fixed-time backstepping controller (FxTBC) with the AFxTDO yields a unified robust control framework that effectively compensates for model uncertainties and external disturbances, while simultaneously ensuring strict fixed-time convergence of the tracking errors.

3.1. Control strategy

The proposed controller synthesis is achieved by integrating a hierarchical fixed-time backstepping architecture with an adaptive fixed-time disturbance observer (AFxTDO) through the following systematic procedure

Step 1. *Hierarchical fixed-time filtered backstepping Controller*

The first translational error variable is expressed as

$$e_1 = \xi - \xi_d \tag{3.1}$$

We select $V_1 = 1/2e_1^T e_1$ as a Lyapunov candidate function. Computing $\dot{V}_1$ results in

$$\dot{V}_1 = e_1^T \left(\upsilon^* - \dot{\xi}_d\right) + e_1^T (\upsilon - \upsilon^*) \tag{3.2}$$

To achieve convergence of e_1, we select υ^* as:

$$\upsilon^* = \dot{\xi}_d - K_1 \mathrm{sig}^{p/q}(e_1) - B_1 \mathrm{sig}^{q/p}(e_1) \tag{3.3}$$

where $K_1 \in \mathbb{R}_+^{3\times3}$ and $B_1 \in \mathbb{R}_+^{3\times3}$ are positive-definite gain matrices, and the positive integers p and q satisfy $p > q$.

The signal υ^* contains fixed-time stabilizing terms and defines the desired behavior for $\dot{\xi}_d$. From equation (3.3), the derivative $\dot{\upsilon}^*$ exhibits a singularity at $e_1 = 0$ when $\dot{e}_1 \neq 0$, owing to the negative fractional power $\frac{p}{q} - 1 < 0$. Such a singularity would produce unbounded control inputs in the subsequent backstepping steps, thereby compromising the practical implementability of the control law. To circumvent this issue, a fixed-time command filter is introduced as:

$$\begin{array}{lcl} \dot{\upsilon}_d & = & -\sigma_\xi^{-1}\mathrm{sig}^{p/q}(\upsilon_d - \upsilon^*) - \sigma_\xi^{-1}\mathrm{sig}^{q/p}(\upsilon_d - \upsilon^*) \\ \upsilon_d(0) & = & \upsilon^*(0) \end{array} \tag{3.4}$$

where υ_d is the filtered variable and $\sigma_\xi^{-1} \in \mathbb{R}^{3\times3}$ denotes a positive-definite design parameter of small magnitude.

Step 2.

The next error is expressed as

$$e_2 = \upsilon - \upsilon_d \tag{3.5}$$

Computing $\dot{e}_2$ gives

$$\dot{e}_2 = \frac{T_z}{m}\mathcal{R}_\eta z_e - g z_e + d_{ext} - \dot{\upsilon}_d \tag{3.6}$$

Disturbances denoted by d_{ext} influence the translational system. These uncertainties are handled via fixed-time estimation and compensation.

Assumption 1. *We impose the boundedness condition $\|d_{ext}\|_\infty \leq H_\xi$ on d_{ext}, where H_ξ is an unknown positive constant.*

3.2. Design of the adaptive fixed-time disturbance observer

For system (3.6), the disturbance estimation law is defined as

$$\begin{aligned} \dot{\hat{e}}_2 &= \frac{T_z}{m}\mathcal{R}_\eta z_e - g z_e + \hat{d}_{ext} - \dot{v}_d \\ \hat{d}_{ext} &= L_1 \mathrm{sig}^{p/q}(\tilde{e}_2) + L_2 \mathrm{sig}^{q/p}(\tilde{e}_2) + \hat{H}\mathrm{sign}(\tilde{e}_2) \end{aligned} \tag{3.7}$$

where the vector $\hat{H} = [\hat{h}_1, \hat{h}_2, \hat{h}_3]$ provides an estimate of $H_\xi = [h_1, h_2, h_3]$. Derivation of the error dynamics yields for each state:

$$\dot{\tilde{e}}_{2i} = -l_{1i}\mathrm{sig}^{p/q}(\tilde{e}_{2i}) - l_{2i}\mathrm{sig}^{q/p}(\tilde{e}_{2i}) - \hat{h}_i \mathrm{sign}(\tilde{e}_{2i}) + d_{ext,i} \tag{3.8}$$

where $i = \{x, y, z\}$.

Theorem 1. *Consider the error dynamics (3.6), and the disturbance observer (3.7), under Assumption 1, selecting the observer gains such that*

$$l_{1i} = k_{1i}\left(\frac{1}{2}\right)^{\frac{p+q}{2q}}, \quad l_{2i} = k_{2i} 6^{\frac{2p}{p-q}} \left(\frac{1}{2}\right)^{\frac{p+q}{2p}} \tag{3.9}$$

where the parameter estimate $\hat{h}_i$ evolves via the adaptation law

$$\begin{cases} \dot{\hat{h}}_i &= r_{0i}|\tilde{e}_{2i}| - k_{1i}\hat{h}_i - r_{1i}\hat{h}_i^{\frac{q}{p}} \\ r_{1i} &= k_{2i}\frac{p+q}{q} \cdot r_{0i}^{\frac{q-p}{2p}} 2^{\frac{p+q}{2p}} \end{cases} \tag{3.10}$$

Then, the observer provides fixed-time convergence for estimating $d_{ext,i}$.

$$T_{ob1} \leq \frac{2q}{k_{1i}\varrho_0(q-p)} + \frac{2p}{k_{2i}\varrho_0(q-p)} \tag{3.11}$$

Proof 1.

$$\mathcal{L}_1 = \frac{1}{2}\tilde{e}_{2i}^2 + \frac{1}{2r_{0i}}\tilde{h}_i^2, \qquad \tilde{h}_i = h_i - \hat{h}_i \tag{3.12}$$

From (3.5)–(3.10), one has

$$\dot{\mathcal{L}}_1 = \tilde{e}_{2i}\left(-l_{1i}\mathrm{sig}^{\frac{p}{q}}(\tilde{e}_{2i}) - l_{2i}\mathrm{sig}^{\frac{q}{p}}(\tilde{e}_{2i}) - \hat{h}_i\mathrm{sign}(\tilde{e}_{2i}) + d_{ext,i}\right) + \frac{1}{r_{0i}}\tilde{h}_i(\dot{h}_i - \dot{\hat{h}}_i) \tag{3.13}$$

Substituting (3.10) into (3.13) and invoking Lemma 4 yields

$$\begin{aligned} \dot{\mathcal{L}}_1 &= \tilde{e}_{2i}\left(-l_{1i}\mathrm{sig}^{\frac{p}{q}}(\tilde{e}_{2i}) - l_{2i}\mathrm{sig}^{\frac{q}{p}}(\tilde{e}_{2i})\right) + \tilde{e}_{2i}d_{ext,i} - \hat{h}_i|\tilde{e}_{2i}| - \frac{1}{r_{0i}}\tilde{h}_i\dot{\hat{h}}_i \\ &\leq -l_{1i}\left(|\tilde{e}_{2i}|^2\right)^{\frac{p+q}{2q}} - l_{2i}6^{\frac{p-q}{2p}}\left(|\tilde{e}_{2i}|^2\right)^{\frac{q+p}{2p}} + \tilde{h}_i|\tilde{e}_{2i}| - \frac{1}{r_{0i}}\tilde{h}_i\dot{\hat{h}}_i \\ &= -l_{1i}\left(|\tilde{e}_{2i}|^2\right)^{\frac{p+q}{2q}} - l_{2i}6^{\frac{p-q}{2p}}\left(|\tilde{e}_{2i}|^2\right)^{\frac{q+p}{2p}} - \frac{\tilde{h}_i}{r_{0i}}\left(\dot{\hat{h}}_i - r_{0i}|\tilde{e}_{2i}|\right) \\ &\leq -l_{1i}\left(|\tilde{e}_{2i}|^2\right)^{\frac{p+q}{2q}} - l_{2i}6^{\frac{p-q}{2p}}\left(|\tilde{e}_{2i}|^2\right)^{\frac{q+p}{2p}} + \frac{k_{1i}}{r_{0i}}\tilde{h}_i\hat{h}_i + \frac{r_{1i}}{r_{0i}}\tilde{h}_i\hat{h}_i^{\frac{q}{p}} \\ &\leq -l_{1i}\left(|\tilde{e}_{2i}|^2\right)^{\frac{p+q}{2q}} - l_{2i}6^{\frac{p-q}{2p}}\left(|\tilde{e}_{2i}|^2\right)^{\frac{q+p}{2p}} - \frac{k_{1i}}{2r_{0i}}\tilde{h}_i^2 + \frac{k_{1i}}{2r_{0i}}h_i^2 + \frac{r_{1i}}{r_{0i}}\tilde{h}_i\hat{h}_i^{\frac{q}{p}} \end{aligned} \tag{3.14}$$

To demonstrate fixed-time convergence of (3.12), the expressions $-\frac{k_{1i}}{2r_{0i}}\tilde{h}_i^2$ and $\frac{r_{1i}}{r_{0i}}\tilde{h}_i\hat{h}_i^{\frac{q}{p}}$ are analyzed using Lemmas 2 and 3, respectively.

Through Lemma 2, defining $z_1 = \frac{\tilde{h}_i^2}{2r_{0i}}$, $z_2 = 1$, $\alpha_1 = \frac{p+q}{2q}$, $\alpha_2 = \frac{q-p}{2q}$ and $\mu = \frac{2q}{p+q}$, one obtains:

$$\left(\frac{\tilde{h}_i^2}{2r_{0i}}\right)^{\frac{p+q}{2q}} \leq \frac{\tilde{h}_i^2}{2r_{0i}} + \left(\frac{q-p}{2q}\right)\mu^{\frac{p+q}{p-q}} \tag{3.15}$$

Invoking Lemma 3 with the definition of $\tilde{h}_i$ results in:

$$\tilde{h}_i\hat{h}_i^{\frac{q}{p}} = \tilde{h}_i\left(h_i - \tilde{h}_i\right)^{\frac{q}{p}} \leq \frac{q}{p+q}\left(h_i^{\frac{q+p}{p}} - \tilde{h}_i^{\frac{q+p}{p}}\right) \tag{3.16}$$

Placing Eqs. (3.15) and (3.16) into Eq. (3.14) leads to

$$\begin{aligned}
\dot{\mathcal{L}}_1 &\leq -l_{1i}\left(|\tilde{e}_{2i}|^2\right)^{\frac{p+q}{2q}} - l_{2i}6^{\frac{p-q}{2p}}\left(|\tilde{e}_{2i}|^2\right)^{\frac{p+q}{2p}} - k_{1i}\left(\frac{\tilde{h}_i^2}{2r_{0i}}\right)^{\frac{p+q}{2q}} + k_{1i}\left(\frac{q-p}{2q}\right)\mu^{\frac{p+q}{p-q}} \\
&\quad + \frac{k_{1i}}{2r_{0i}}h_i^2 + \frac{r_{1i}}{r_{0i}}\cdot\frac{q}{p+q}\left(h_i^{\frac{p+q}{p}} - \tilde{h}_i^{\frac{p+q}{p}}\right) \\
&\leq -l_{1i}\left(|\tilde{e}_{2i}|^2\right)^{\frac{p+q}{2q}} - l_{2i}6^{\frac{p-q}{2p}}\left(|\tilde{e}_{2i}|^2\right)^{\frac{p+q}{2p}} - k_{1i}\left(\frac{\tilde{h}_i^2}{2r_{0i}}\right)^{\frac{p+q}{2q}} + k_{1i}\left(\frac{q-p}{2q}\right)\mu^{\frac{p+q}{p-q}} + \frac{k_{1i}}{2r_{0i}}h_i^2 + \frac{r_{1i}}{r_{0i}}\frac{q}{p+q}h_i^{\frac{q+p}{p}} \\
&\quad - r_{1i}\frac{q}{p+q}\left(\frac{\tilde{h}_i^2}{2r_{0i}}\right)^{\frac{p+q}{2p}}\cdot 2^{-\frac{p+q}{2p}}\cdot r_{0i}^{\frac{p-q}{2p}} \\
&\leq -l_{1i}(|\tilde{e}_{2i}|^2)^{\frac{p+q}{2q}} - l_{2i}6^{\frac{p-q}{2p}}\left(|\tilde{e}_{2i}|^2\right)^{\frac{p+q}{2p}} - k_{1i}\left(\frac{\tilde{h}_i^2}{2r_{0i}}\right)^{\frac{p+q}{2q}} - r_{1i}\frac{q}{p+q}\left(\frac{\tilde{h}_i^2}{2r_{0i}}\right)^{\frac{p+q}{2p}}\cdot 2^{-\frac{p+q}{2p}}\cdot r_{0i}^{\frac{p-q}{2p}} + \vartheta_1
\end{aligned} \tag{3.17}$$

where ϑ_1 is defined as

$$\vartheta_1 = \frac{k_{1i}}{2r_{0i}}h_i^2 + \frac{r_{1i}}{r_{0i}}\frac{q}{p+q}h_i^{\frac{q+p}{p}} + k_{1i}\left(\frac{q-p}{2q}\right)\mu^{\frac{p+q}{p-q}} \tag{3.18}$$

From Eqs. (3.9) and (3.10) substituted into Eq. (3.17), and using Lemma 4, one obtains

$$\begin{aligned}
\dot{\mathcal{L}}_1 &\leq -k_{1i}\left(\tfrac{1}{2}|\tilde{e}_{2i}|^2\right)^{\frac{p+q}{2q}} - k_{2i}\left(\tfrac{1}{2}|\tilde{e}_{2i}|^2\right)^{\frac{p+q}{2p}} - k_{1i}\left(\frac{\tilde{h}_i^2}{2r_{0i}}\right)^{\frac{p+q}{2q}} - k_{2i}\left(\frac{\tilde{h}_i^2}{2r_{0i}}\right)^{\frac{p+q}{2p}} + \vartheta_1 \\
&\leq -k_{1i}\left(\tfrac{1}{2}|\tilde{e}_{2i}|^2 + \frac{\tilde{h}_i^2}{2r_{0i}}\right)^{\frac{p+q}{2q}} - k_{2i}\left(\tfrac{1}{2}|\tilde{e}_{2i}|^2 + \frac{\tilde{h}_i^2}{2r_{0i}}\right)^{\frac{p+q}{2p}} \\
&\leq -k_{1i}V_1^{\frac{p+q}{2q}} - k_{2i}V_1^{\frac{p+q}{2p}} + \vartheta_1
\end{aligned} \tag{3.19}$$

The parameter ϑ_1 depends on the observer design gains and is therefore globally bounded. Let $\chi_1 = [\tilde{e}_{2i}, \tilde{h}_i]^T$ represent the observation error vector. By Lemma 1, the vector χ_1 converges in fixed time to a compact set centered at the origin with radius

$$\min\left\{\left(\frac{\vartheta_1}{(1-\varrho_0)k_{1i}}\right)^{\frac{2q}{p+q}}, \left(\frac{\vartheta_1}{(1-\varrho_0)k_{2i}}\right)^{\frac{2p}{p+q}}\right\}, \quad 0 < \varrho_0 < 1 \tag{3.20}$$

where the convergence time T_{ob1} satisfies the upper bound

$$T_{ob1} \leq \frac{2q}{k_{1i}\varrho_0(q-p)} + \frac{2p}{k_{2i}\varrho_0(q-p)} \tag{3.21}$$

Thus, for $t_1 \geq T_{ob1}$, system (3.6) becomes

$$\dot{e}_2 = \frac{T_z}{m}\mathcal{R}_\eta z_e - g z_e + \hat{d}_{ext} - \dot{\upsilon}_d \tag{3.22}$$

Consider the augmented Lyapunov function as

$$V_2 = V_1 + \frac{1}{2}e_2^T e_2 + \frac{1}{2}y_1^T y_1 \tag{3.23}$$

where the filter error is $y_1 = \upsilon_d - \upsilon^*$. Computing $\dot{V}_2$ gives

$$\dot{V}_2 = e_1^T(e_2 + y_1) - \sum_{i=1}^{3} k_{1i}|e_{1i}|^{\frac{p+q}{q}} - \sum_{i=1}^{3} b_{1i}|e_{1i}|^{\frac{p+q}{p}} + y_1^T(\dot{\upsilon} - \dot{\upsilon}^*) + e_2^T\left(u_\xi + \hat{d}_{ext} - \dot{\upsilon}_d\right) + e_2^T\left(\frac{T_z}{m}R_\eta z_e - g z_e - u_\xi\right) \tag{3.24}$$

where

$$u_\xi = \frac{T_z}{m}\mathcal{R}_\eta^d z_e - g z_e \tag{3.25}$$

The outer-loop controller synthesizes the required thrust command T_z^d and desired rotation matrix R_η^d. Assuming ideal thrust response ($T_z = T_z^d$), these signals enable accurate path tracking.

The control input is chosen as follows:

$$u_\xi = \dot{\upsilon}_d - \hat{d}_{ext} - e_1 - K_2 \mathrm{sig}^{p/q}(e_2) - B_2 \mathrm{sig}^{q/p}(e_2) \tag{3.26}$$

where the control gains $K_2 \in \mathbb{R}_+^{3\times3}$ and $B_2 \in \mathbb{R}_+^{3\times3}$ are design parameters. The coupling term is addressed in the following step. Using (3.26) in (3.24) results in

$$\dot{V}_2 = e_1^T y_1 - \sum_{i=1}^{3} k_{1i}|e_{1i}|^{\frac{p+q}{q}} - \sum_{i=1}^{3} b_{1i}|e_{1i}|^{\frac{p+q}{p}} - \sum_{i=1}^{3} k_{2i}|e_{2i}|^{\frac{p+q}{q}} - \sum_{i=1}^{3} b_{2i}|e_{2i}|^{\frac{p+q}{p}} + y_1^T\left(-\sigma_\xi^{-1}\left[\mathrm{sig}^{\frac{p}{q}}(y_1) + \mathrm{sig}^{\frac{q}{p}}(y_1)\right] - \dot{\upsilon}^*\right) \tag{3.27}$$

Assumption 2. *Suppose there is a constant $\Delta_{\xi,i} > 0$ for which*

$$|\dot{\upsilon}_i^*| \leq \Delta_{\xi,i} \tag{3.28}$$

Applying Lemma 5 yields:

$$|e_{1,i}||y_{1,i}| \leq \frac{\Lambda_{1,i}^{\frac{p+q}{q}}}{\frac{p}{q}+1}|e_{1,i}|^{\frac{p+q}{q}} + \frac{\Lambda_{1,i}^{-\frac{p+q}{p}}}{\frac{q}{p}+1}|y_{1,i}|^{\frac{p+q}{p}} \tag{3.29}$$

$$|y_{1,i}||\dot{\upsilon}_i^*| \leq |y_{1,i}|\,|\Delta_{\xi,i}| \leq \frac{\Lambda_{2,i}^{\frac{p+q}{q}}}{\frac{p}{q}+1}|y_{1,i}|^{\frac{p+q}{q}} + \frac{\Lambda_{2,i}^{-\frac{p+q}{p}}}{\frac{q}{p}+1}\Delta_{\xi,i}^{\frac{p+q}{p}} \tag{3.30}$$

Applying (3.29) and (3.30) to (3.27) produces

$$\begin{aligned}\dot{V}_2 \leq & -\sum_{i=1}^{3}\left(k_{1,i}-\frac{\Lambda_{1,i}^{\frac{p+q}{q}}}{\frac{p}{q}+1}\right)|e_{1,i}|^{\frac{p+q}{q}}-\sum_{i=1}^{3}b_{1,i}|e_{1,i}|^{\frac{p+q}{p}}\\ & -\sum_{i=1}^{3}k_{2,i}|e_{2,i}|^{\frac{p+q}{q}}-\sum_{i=1}^{3}b_{2,i}|e_{2,i}|^{\frac{p+q}{p}}\\ & -\sum_{i=1}^{3}\left(\frac{1}{\sigma_{\xi,i}}-\frac{\Lambda_{2,i}^{\frac{p+q}{q}}}{\frac{p}{q}+1}\right)|y_{1,i}|^{\frac{p+q}{q}}-\sum_{i=1}^{3}\left(\frac{1}{\sigma_{\xi,i}}-\frac{\Lambda_{1,i}^{-\frac{p+q}{p}}}{\frac{q}{p}+1}\right)|y_{1,i}|^{\frac{p+q}{p}}\\ & +\sum_{i=1}^{3}\frac{\Lambda_{2,i}^{-\frac{p+q}{p}}}{\frac{q}{p}+1}\Delta_{\xi,i}^{\frac{p+q}{p}}\end{aligned} \tag{3.31}$$

The gains are configured such that

$$\begin{cases}k_{1,i}>\dfrac{\Lambda_{1,i}^{\frac{p+q}{q}}}{\frac{p}{q}+1},\\ \dfrac{1}{\sigma_{\xi,i}}>\max\left\{\dfrac{\Lambda_{1,i}^{-\frac{p+q}{p}}}{\frac{q}{p}+1},\ \dfrac{\Lambda_{2,i}^{\frac{p+q}{q}}}{\frac{p}{q}+1}\right\}\end{cases} \tag{3.32}$$

Based on (3.32), we obtain:

$$\dot{V}_2\leq-\tilde{\gamma}_1\left(\left(\tfrac{1}{2}\|e_1\|^2\right)^{\frac{p+q}{2q}}+\left(\tfrac{1}{2}\|e_2\|^2\right)^{\frac{p+q}{2q}}+\left(\tfrac{1}{2}\|y_1\|^2\right)^{\frac{p+q}{2q}}\right)-\tilde{\gamma}_2\left(\left(\tfrac{1}{2}\|e_1\|^2\right)^{\frac{p+q}{2p}}+\left(\tfrac{1}{2}\|e_2\|^2\right)^{\frac{p+q}{2p}}+\left(\tfrac{1}{2}\|y_1\|^2\right)^{\frac{p+q}{2p}}\right)+\gamma_3 \tag{3.33}$$

where $\tilde{\gamma}_1=2^{\frac{p+q}{2q}}\bar{\gamma}_1$, $\tilde{\gamma}_2=2^{\frac{p+q}{2p}}\bar{\gamma}_2$, $\gamma_3>0$.

$$\begin{aligned}\bar{\gamma}_1=\min\Bigg(&k_{1,1}-\frac{\Lambda_{1,1}^{\frac{p+q}{q}}}{\frac{p}{q}+1},\ k_{1,2}-\frac{\Lambda_{1,2}^{\frac{p+q}{q}}}{\frac{p}{q}+1},\ k_{1,3}-\frac{\Lambda_{1,3}^{\frac{p+q}{q}}}{\frac{p}{q}+1},\ k_{2,1},\ k_{2,2},\ k_{2,3},\frac{1}{\sigma_{\xi,1}}-\frac{\Lambda_{2,1}^{\frac{p+q}{q}}}{\frac{p}{q}+1},\ \frac{1}{\sigma_{\xi,2}}-\frac{\Lambda_{2,2}^{\frac{p+q}{q}}}{\frac{p}{q}+1},\\ &\frac{1}{\sigma_{\xi,3}}-\frac{\Lambda_{2,3}^{\frac{p+q}{q}}}{\frac{p}{q}+1}\Bigg)\end{aligned} \tag{3.34}$$

$$\bar{\gamma}_2=\min\left(\beta_{1,1},\ \beta_{1,2},\ \beta_{1,3},\ \beta_{2,1},\ \beta_{2,2},\ \beta_{2,3},\frac{1}{\sigma_{\xi,1}}-\frac{\Lambda_{1,1}^{-\frac{p+q}{p}}}{\frac{q}{p}+1},\ \frac{1}{\sigma_{\xi,2}}-\frac{\Lambda_{1,2}^{-\frac{p+q}{p}}}{\frac{q}{p}+1},\ \frac{1}{\sigma_{\xi,3}}-\frac{\Lambda_{1,3}^{-\frac{p+q}{p}}}{\frac{q}{p}+1}\right) \tag{3.35}$$

$$\gamma_3=\sum_{i=1}^{3}\frac{\Lambda_{2,i}^{-\frac{p+q}{p}}}{\frac{q}{p}+1}\Delta_{\xi,i}^{\frac{p+q}{p}} \tag{3.36}$$

By invoking Lemma 2, we rewrite (3.33) as

$$\dot{V}_2\leq-\tilde{\gamma}_1V_2^{\frac{p+q}{2q}}-\tilde{\gamma}_2V_2^{\frac{p+q}{2p}}+\gamma_3 \tag{3.37}$$

Define the error state $\chi_2 = \left[e_1\ e_2\ y_1\right]^T$ for the outer-loop closed-loop system. From Lemma 1, χ_2 reaches, within a fixed settling time, a small neighborhood of the origin with radius

$$\min\left(\tilde{\gamma}_1^{-\frac{2q}{p+q}}\left(\frac{\gamma_3}{1-\phi_0}\right)^{\frac{2q}{p+q}},\ \tilde{\gamma}_2^{-\frac{2p}{p+q}}\left(\frac{\gamma_3}{1-\phi_0}\right)^{\frac{2p}{p+q}}\right) \tag{3.38}$$

The fixed settling time is $\bar{T}_1 = T_{\text{ob1}} + T_1$, where T_1 is bounded by

$$T_1 \leq \frac{1}{\tilde{\gamma}_1\,\phi_0}\frac{2q}{q-p} + \frac{1}{\tilde{\gamma}_2\,\phi_0}\frac{2p}{q-p} \tag{3.39}$$

for $\phi_0 \in (0, 1]$. It is worth noting that the time bound in (3.39) remains constant regardless of initial error states.

From the outer control u_ξ, we obtain the reference attitude η_d. The error is then defined by

$$e_\epsilon = u_\xi - \frac{T_z}{m}\mathcal{R}_\eta z_e + g z_e \tag{3.40}$$

Classical backstepping typically introduces additional auxiliary errors e_ϵ, which increase the complexity of the design and hinder practical implementation. By employing a hierarchical backstepping strategy, we decouple the position and attitude dynamics into distinct subsystems: the attitude dynamics evolve independently, whereas position tracking depends on the desired rotation matrix $\mathcal{R}_\eta^d$, thereby simplifying the overall control architecture and reducing the associated computational burden.

Expression (3.25) yields the commanded force norm and rotation matrix $\mathcal{R}_\eta^d$ according to:

$$\begin{cases} T_z = m\sqrt{u_x^2 + u_y^2 + (u_z + g)^2}, \\ \phi_d = \arcsin\left[\frac{m}{T_z}\left(u_x \sin\psi_d - u_y \cos\psi_d\right)\right], \\ \theta_d = \arcsin\left[\frac{m}{T_z \cos\phi_d}\left(u_x \cos\psi_d + u_y \sin\psi_d\right)\right]. \end{cases} \tag{3.41}$$

Step 3.

A new error variable is then defined as

$$e_3 = \eta - \eta_d \tag{3.42}$$

Let us take $\eta = \eta_d + e_3$ and then the vector $\frac{T_z}{m}\mathcal{R}_\eta z_e$ can be rewritten as

$$\frac{T_z}{m}\mathcal{R}_\eta z_e = \frac{T_z}{m}\mathcal{R}_\eta^d z_e + \frac{1}{m}h(\eta_d, e_3) \tag{3.43}$$

The vector $h(\eta_d, e_3)$ represents the interconnection term between the translation and rotation dynamics and can be found in [8].

Substituting (3.43) into (3.40), one gets

$$e_\epsilon = \frac{1}{m}h(\eta_d, e_3) \tag{3.44}$$

According to [8], it can be readily shown that the interconnection term $h(\eta_d, e_3)$ is bounded. Furthermore, when $e_3 = 0$, it follows that $h(\eta_d, 0) = 0$, which implies $e_\epsilon = 0$.

Consider now the following Lyapunov function:

$$V_3 = \frac{1}{2} e_3^T e_3 \tag{3.45}$$

Its derivative is:

$$\dot{V}_3 = e_3^T(\omega^* - \dot{\eta}_d) + e_3^T(\omega - \omega^*) \tag{3.46}$$

Considering the virtual control input

$$\omega^* = \dot{\eta}_d - K_3 \mathrm{sig}^{p/q}(e_3) - B_3 \mathrm{sig}^{q/p}(e_3) \tag{3.47}$$

where $K_3 \in \mathbb{R}_+^{3\times3}$ and $B_3 \in \mathbb{R}_+^{3\times3}$, and substituting (3.47) into (3.46) yields

$$\begin{aligned} \dot{V}_3 &= -e_3^T K_3 \mathrm{sig}^{\frac{p}{q}}(e_3) - e_3^T B_3 \mathrm{sig}^{\frac{q}{p}}(e_3) + e_3^T(\omega - \omega^*) \\ &= -\sum_{i=1}^{3} k_{3,i} |e_{3,i}|^{\frac{p+q}{q}} - \sum_{i=1}^{3} b_{3,i} |e_{3,i}|^{\frac{p+q}{p}} + e_3^T(\omega - \omega^*) \end{aligned} \tag{3.48}$$

We introduce a new state variable ω_d and the dynamics of the new state variable satisfy

$$\begin{cases} \dot{\omega}_d &= -\sigma_\eta^{-1}\left[\mathrm{sig}^{p/q}(\omega_d - \omega^*) + \mathrm{sig}^{q/p}(\omega_d - \omega^*)\right] \\ \omega_d(0) &= \omega^*(0) \end{cases} \tag{3.49}$$

where $\sigma_\eta \in \mathbb{R}^{3\times3}$ is a designed parameter.

Step 4.

Consider the fourth error as

$$e_4 = \omega - \omega_d \tag{3.50}$$

Differentiating (3.50) with respect to time, we get

$$\dot{e}_4 = \tau - C(\eta, \dot{\eta})\,\dot{\eta} + \tau_{ext} - \dot{\omega}_d \tag{3.51}$$

Rotational dynamics are subject to disturbances represented by τ_{ext}. These perturbations will be estimated and rejected using a fixed-time observation scheme.

Assumption 3. *We impose the boundedness condition $\|\tau_{ext}\|_\infty \leq \lambda$ on τ_{ext}, where λ is an unknown positive constant.*

3.3. Design of adaptive fixed-time disturbance observer

The disturbance observer for system (3.51) is governed by

$$\begin{aligned} \dot{\hat{e}}_4 &= \tau - C(\eta, \dot{\eta})\,\dot{\eta} + \hat{\tau}_{ext} - \dot{\omega}_d \\ \hat{\tau}_{ext} &= L_3 \mathrm{sig}^{p/q}(\tilde{e}_4) + L_4 \mathrm{sig}^{q/p}(\tilde{e}_4) + \hat{\lambda}\mathrm{sign}(\tilde{e}_4) \end{aligned} \tag{3.52}$$

where $\hat{\lambda} = [\hat{\lambda}_1, \hat{\lambda}_2, \hat{\lambda}_3]$ is an estimate of $\lambda = [\lambda_1, \lambda_2, \lambda_3]$. The observer error dynamics can then be derived for each state as

$$\dot{\tilde{e}}_{4j} = -l_{3j} \mathrm{sig}^{p/q}(\tilde{e}_{4j}) - l_{4j} \mathrm{sig}^{q/p}(\tilde{e}_{4j}) - \hat{\lambda}_j \mathrm{sign}(\tilde{e}_{4j}) + \tau_{ext,j} \tag{3.53}$$

where $j = \{\phi, \theta, \psi\}$.

Theorem 2. *Consider the error system (3.51) and the designed observer (3.52) under Assumption 3. If the observer gains are selected as*

$$l_{3j} = k_{3j}\left(\frac{1}{2}\right)^{\frac{p+q}{2q}}, \quad l_{4j} = k_{4j}6^{\frac{2p}{p-q}}\left(\frac{1}{2}\right)^{\frac{p+q}{2p}} \tag{3.54}$$

and the estimate $\hat{\lambda}_j$ updated by the adaptive law

$$\begin{cases} \dot{\hat{\lambda}}_j &= r_{0j}|\tilde{e}_{4j}| - k_{3j}\hat{\lambda}_j - r_{1j}\hat{\lambda}_j^{\frac{q}{p}} \\ r_{1j} &= k_{4j}\frac{p+q}{q}\cdot r_{0j}^{\frac{q-p}{2p}} 2^{\frac{p+q}{2p}} \end{cases} \tag{3.55}$$

then the observer guarantees estimation of $\tau_{ext,j}$ within a fixed time

$$T_{ob2} \leq \frac{2q}{k_{3j}\rho_0(q-p)} + \frac{2p}{k_{4j}\rho_0(q-p)} \tag{3.56}$$

where $0 < \rho_0 < 1$.

Proof 2.

Consistent with the findings in (3.12)–(3.20), provided that the observer gains meet the conditions specified in Theorem 2, state $\tilde{e}_4$ converges to the origin uniformly in fixed time.

Consequently, after $T_2 > T_{ob2}$, expression (3.51) becomes

$$\dot{e}_4 = \tau - C(\eta,\dot{\eta})\,\dot{\eta} + \hat{\tau}_{ext} - \dot{\omega}_d \tag{3.57}$$

Consider the augmented Lyapunov function candidate

$$V_4 = V_3 + \frac{1}{2}e_4^T e_4 + \frac{1}{2}y_2^T y_2 \tag{3.58}$$

where $y_2 = \omega_d - \omega^*$. Differentiating V_4 with respect to time yields

$$\begin{aligned} \dot{V}_4 &= e_3^T(e_4 + y_2) - e_3^T K_3 \mathrm{sig}^{\frac{p}{q}}(e_3) - e_3^T B_3 \mathrm{sig}^{\frac{q}{p}}(e_3) + e_4^T(\tau - C(\eta,\dot{\eta})\,\dot{\eta} + \hat{\tau}_{ext} - \dot{\omega}_d) \\ &\quad - y_2^T\sigma_\eta^{-1}\left(\mathrm{sig}^{\frac{p}{q}}(y_2) + \mathrm{sig}^{\frac{q}{p}}(y_2)\right) - y_2^T\dot{\omega}^* \end{aligned} \tag{3.59}$$

The stabilization of e_4 can be ensured by introducing the control input τ:

$$\tau = -e_3 + \dot{\omega}_d - \hat{\tau}_{ext} - K_4\mathrm{sig}^{p/q}(e_4) - B_4\mathrm{sig}^{q/p}(e_4) \tag{3.60}$$

where $K_4 \in \mathbb{R}_+^{3\times3}$ and $B_4 \in \mathbb{R}_+^{3\times3}$. Substituting (3.60) into (3.59), we get

$$\begin{aligned} \dot{V}_4 &= e_3^T y_2 - e_3^T K_3 \mathrm{sig}^{\frac{p}{q}}(e_3) - e_3^T B_3 \mathrm{sig}^{\frac{q}{p}}(e_3) - e_4^T K_4 \mathrm{sig}^{\frac{p}{q}}(e_4) - e_4^T B_4 \mathrm{sig}^{\frac{q}{p}}(e_4) \\ &\quad - y_2^T\sigma_\eta^{-1}\left(\mathrm{sig}^{\frac{p}{q}}(y_2) + \mathrm{sig}^{\frac{q}{p}}(y_2)\right) - y_2^T\dot{\omega}^* \\ &\leq -\sum_{i=1}^{3} k_{3,i}|e_{3,i}|^{\frac{p+q}{q}} - \sum_{i=1}^{3} b_{3,i}|e_{3,i}|^{\frac{p+q}{p}} - \sum_{i=1}^{3} k_{4,i}|e_{4,i}|^{\frac{p+q}{q}} - \sum_{i=1}^{3} b_{4,i}|e_{4,i}|^{\frac{p+q}{p}} \\ &\quad - \sum_{i=1}^{3}\frac{1}{\sigma_{\eta,i}}\left(|y_{2,i}|^{\frac{p+q}{q}} + |y_{2,i}|^{\frac{p+q}{p}}\right) + \sum_{i=1}^{3}|e_{3,i}||y_{2,i}| + \sum_{i=1}^{3}|y_{2,i}||\dot{\omega}_i^*| \end{aligned} \tag{3.61}$$

Assumption 4. *Suppose there is a constant $\Delta_{\eta,i} > 0$ for which*

$$|\dot{\omega}_i^*| \leq \Delta_{\eta,i} \tag{3.62}$$

According to Lemma 5 and Assumption 4, we have:

$$\begin{aligned} |e_{3,i}|\,|y_{2,i}| &\leq \tfrac{p}{p+q}\,\Lambda_{3,i}^{\frac{p}{q}+1}|e_{3,i}|^{\frac{p+q}{q}} + \tfrac{q}{p+q}\,\Lambda_{3,i}^{-\frac{q}{p}-1}|y_{2,i}|^{\frac{p+q}{p}} \\ |y_{2,i}|\,|\dot{\omega}_i^*| &\leq |y_{2,i}|\,\Delta_{\eta,i} \leq \tfrac{p}{p+q}\,\Lambda_{4,i}^{\frac{p}{q}+1}|y_{2,i}|^{\frac{p+q}{q}} + \tfrac{q}{p+q}\,\Lambda_{4,i}^{-\frac{q}{p}-1}\Delta_{\eta,i}^{\frac{p+q}{p}} \end{aligned} \tag{3.63}$$

Substituting (3.63) into (3.61), one gets:

$$\begin{aligned} \dot{V}_4 \leq\ & -\sum_{i=1}^{3}\left(k_{3,i} - \frac{p}{p+q}\Lambda_{3,i}^{\frac{p}{q}+1}\right)|e_{3,i}|^{\frac{p+q}{q}} - \sum_{i=1}^{3} b_{3,i}|e_{3,i}|^{\frac{p+q}{p}} - \sum_{i=1}^{3} k_{4,i}|e_{4,i}|^{\frac{p+q}{q}} - \sum_{i=1}^{3} b_{4,i}|e_{4,i}|^{\frac{p+q}{p}} \\ & -\sum_{i=1}^{3}\left(\frac{1}{\sigma_{\eta,i}} - \frac{p}{p+q}\Lambda_{4,i}^{\frac{p}{q}+1}\right)|y_{2,i}|^{\frac{p+q}{q}} - \sum_{i=1}^{3}\left(\frac{1}{\sigma_{\eta,i}} - \frac{q}{p+q}\Lambda_{3,i}^{-\frac{q}{p}-1}\right)|y_{2,i}|^{\frac{p+q}{p}} + \sum_{i=1}^{3}\frac{q}{p+q}\Lambda_{4,i}^{-\frac{q}{p}-1}\Delta_{\eta,i}^{\frac{p+q}{p}} \end{aligned}$$

The design parameters are carefully chosen to ensure that

$$k_{3,i} > \frac{p}{p+q}\,\Lambda_{3,i}^{\frac{p}{q}+1} \tag{3.64}$$

$$\frac{1}{\sigma_{\eta,i}} > \max\left\{\frac{p}{p+q}\,\Lambda_{4,i}^{\frac{p}{q}+1},\ \ \frac{q}{p+q}\,\Lambda_{3,i}^{-\frac{q}{p}-1}\right\} \tag{3.65}$$

It can be concluded from (3.64) that:

$$\dot{V}_4 \leq -\bar{\gamma}_7\left(\sum_{i=1}^{3}|e_{3,i}|^{\frac{p+q}{q}} + \sum_{i=1}^{3}|e_{4,i}|^{\frac{p+q}{q}} + \sum_{i=1}^{3}|y_{2,i}|^{\frac{p+q}{q}}\right) - \bar{\gamma}_8\left(\sum_{i=1}^{3}|e_{3,i}|^{\frac{p+q}{p}} + \sum_{i=1}^{3}|e_{4,i}|^{\frac{p+q}{p}} + \sum_{i=1}^{3}|y_{2,i}|^{\frac{p+q}{p}}\right) + \gamma_9 \tag{3.66}$$

where

$$\bar{\gamma}_7 = \min\left\{k_{3,1} - \frac{p}{p+q}\Lambda_{3,1}^{\frac{p}{q}+1},\ k_{3,2} - \frac{p}{p+q}\Lambda_{3,2}^{\frac{p}{q}+1},\ k_{3,3} - \frac{p}{p+q}\Lambda_{3,3}^{\frac{p}{q}+1},\ k_{4,1},\ k_{4,2},\ k_{4,3},\right. \tag{3.67}$$

$$\left.\frac{1}{\sigma_{\eta,1}} - \frac{p}{p+q}\Lambda_{3,1}^{\frac{p}{q}+1},\ \frac{1}{\sigma_{\eta,2}} - \frac{p}{p+q}\Lambda_{3,2}^{\frac{p}{q}+1},\ \frac{1}{\sigma_{\eta,3}} - \frac{p}{p+q}\Lambda_{3,3}^{\frac{p}{q}+1}\right\} \tag{3.68}$$

$$\bar{\gamma}_8 = \min\left\{b_{3,1},\ b_{3,2},\ b_{3,3},\ b_{4,1},\ b_{4,2},\ b_{4,3},\ \frac{1}{\sigma_{\eta,1}} - \frac{q}{p+q}\Lambda_{3,1}^{-\frac{q}{p}-1},\ \frac{1}{\sigma_{\eta,2}} - \frac{q}{p+q}\Lambda_{3,2}^{-\frac{q}{p}-1},\ \frac{1}{\sigma_{\eta,3}} - \frac{q}{p+q}\Lambda_{3,3}^{-\frac{q}{p}-1}\right\} \tag{3.69}$$

$$\gamma_9 = \sum_{i=1}^{3}\frac{q}{p+q}\Lambda_{4,i}^{-\frac{q}{p}-1}|\Delta_{\eta,i}|^{\frac{p+q}{p}} \tag{3.70}$$

The expression (3.66) can be transformed into

$$\dot{V}_4 \leq -\tilde{\gamma}_7\left[\left(\tfrac{1}{2}\|e_3\|^2\right)^{\frac{p+q}{2q}} + \left(\tfrac{1}{2}\|e_4\|^2\right)^{\frac{p+q}{2q}} + \left(\tfrac{1}{2}\|y_2\|^2\right)^{\frac{p+q}{2q}}\right] - \tilde{\gamma}_8\left[\left(\tfrac{1}{2}\|e_3\|^2\right)^{\frac{p+q}{2p}} + \left(\tfrac{1}{2}\|e_4\|^2\right)^{\frac{p+q}{2p}} + \left(\tfrac{1}{2}\|y_2\|^2\right)^{\frac{p+q}{2p}}\right] + \gamma_9$$

where $\tilde{\gamma}_7 = 2^{\frac{p+q}{2q}}\,\bar{\gamma}_7, \tilde{\gamma}_8 = 2^{\frac{p+q}{2p}}\,\bar{\gamma}_8$. Using Lemma 1 then leads to the following expression:

$$\dot{V}_4 \leq -\tilde{\gamma}_7\, V_4^{\frac{p+q}{2q}} - \tilde{\gamma}_8\, V_4^{\frac{p+q}{2p}} + \gamma_9 \tag{3.71}$$

Consider $\chi_3 = \begin{bmatrix} e_3 & e_4 & y_2 \end{bmatrix}^T$ as the error vector of the closed-loop control of the roll and pitch subsystem. According to Lemma 2, the error vector χ_3 will converge in fixed time to an arbitrarily small neighborhood of the origin given by

$$\min\left\{\tilde{\gamma}_7^{\frac{2q}{p+q}}\left(\frac{\gamma_9}{1-\alpha_0}\right)^{\frac{2q}{p+q}},\ \tilde{\gamma}_8^{-\frac{2p}{p+q}}\left(\frac{\gamma_9}{1-\alpha_0}\right)^{\frac{2p}{p+q}}\right\} \tag{3.72}$$

within a predesigned settling time

$$T_3 = \max\{T_1, T_2\}$$

where T_2 is bounded by

$$T_2 \leq \frac{1}{\tilde{\gamma}_7\,\alpha_0}\frac{2q}{q-p} + \frac{1}{\tilde{\gamma}_8\,\alpha_0}\frac{2p}{q-p} \tag{3.73}$$

Clearly, it is observed that the upper bound of the convergence time in (3.73) is independent of the initial tracking errors and the initial filtering errors.

3.4. Closed-loop dynamics

Applying the control strategies (3.3) and (3.26) to the position subsystem in (2.6), we obtain the closed-loop error representation:

$$\begin{aligned} \dot{e}_1 &= -K_1 \mathrm{sig}^{\frac{p}{q}}(e_1) - B_1 \mathrm{sig}^{\frac{q}{p}}(e_1) + e_2 + y_1 \\ \dot{e}_2 &= -K_2 \mathrm{sig}^{\frac{p}{q}}(e_2) - B_2 \mathrm{sig}^{\frac{q}{p}}(e_2) - e_1 + e_\varepsilon \\ y_1 &= \upsilon_d - \upsilon^* \end{aligned} \tag{3.74}$$

We select the Lyapunov candidate as

$$V_2 = \frac{1}{2}\, e_1^{\mathrm{T}} e_1 + \frac{1}{2}\, e_2^{\mathrm{T}} e_2 + \frac{1}{2}\, y_1^{\mathrm{T}} y_1 \tag{3.75}$$

whose time derivative satisfies

$$\dot{V}_2 \leq -\tilde{\gamma}_4\, V_2^{\frac{p+q}{2q}} - \tilde{\gamma}_5\, V_2^{\frac{p+q}{2p}} + \gamma_6 + e_2^{\mathrm{T}} e_\epsilon \tag{3.76}$$

For the attitude subsystem, the closed-loop error coordinates take the form:

$$\begin{aligned} \dot{e}_3 &= -K_3 \mathrm{sig}^{\frac{p}{q}}(e_3) - B_3 \mathrm{sig}^{\frac{q}{p}}(e_3) + e_4 + y_2 \\ \dot{e}_4 &= -K_4 \mathrm{sig}^{\frac{p}{q}}(e_4) - B_4 \mathrm{sig}^{\frac{q}{p}}(e_4) - e_3 \\ y_2 &= \omega_d - \omega^* \end{aligned} \tag{3.77}$$

The associated Lyapunov function is defined by

$$V_4 = \frac{1}{2} e_3^{\mathrm{T}} e_3 + \frac{1}{2} e_4^{\mathrm{T}} e_4 + \frac{1}{2} y_2^{\mathrm{T}} y_2 \tag{3.78}$$

with derivative bounded by

$$\dot{V}_4 \leq -\tilde{\gamma}_7 V_4^{\frac{p+q}{2q}} - \tilde{\gamma}_8 V_4^{\frac{p+q}{2p}} + \gamma_9 \tag{3.79}$$

Given that e_3 converges to zero within the guaranteed prescribed time bound, the interconnection term e_ϵ vanishes identically by virtue of equations (3.42) and (3.44). Consequently, the overall control structure exhibits a cascade configuration: the position error dynamics (3.74) constitute the outer loop, while the orientation error dynamics (3.77) form the inner loop. By invoking Lemma 1 to (3.77), it is concluded that the attitude subsystem achieves practical fixed-time stability. Accordingly, the variables e_1, e_2, and y_1 enter a neighborhood of the origin as defined in (3.5) within a fixed time bound. An identical line of reasoning applied to the translational subsystem (3.74) establishes its practical fixed-time stability. It is worth noting that the coupling term e_ϵ is completely eliminated once e_3 converges to the origin.

4. Numerical simulations

This section presents a series of simulations, conducted using MATLAB/Simulink, to assess both the effectiveness and robustness of the developed nonlinear cascade filtered fixed-time backstepping controller combined with a novel adaptive disturbance observer. The quadrotor parameters are given as follows [27]: $m = 0.468$ kg, $l = 0.225$ m. The nominal inertia matrix is $J_0 = \mathrm{diag}(J_x, J_y, J_z) = \mathrm{diag}(4.856, 4.856, 8.801) \times 10^{-3}$ kg $\cdot$ m^2, $J_r = 3.357 \times 10^{-5}$ kg $\cdot$ m^2, $\varrho = 2.98 \times 10^{-6}$, $\bar{\varrho} = 1.14 \times 10^{-7}$. A summary of the control parameters is given in Table 1.

Table 1. Controllers and observer parameters.

Control Algorithm	**Controller Parameters**	**Observer Parameters**
AFxTDOBC	$a_{1,i} = 0.75$, $b_{1,i} = 1.1$, $a_{2,i} = b_{2,i} = 1.5$, $p/q = 0.6$, $\sigma_{1,i} = 0.1$, $i = \{\theta, \psi\}$	$k_{1i} = 1.5, k_{2i} = 1.2, r_0 = 10$, $p/q = 0.6$
ESOBC	$a_{1,i} = 1.5$, $a_{2,i} = 2$	$k_{1i} = 2$, $k_{2i} = 5$, $k_{3i} = 10$
FTBC	$a_{1,i} = 1.5$, $a_{2,i} = 2$, $\alpha_i = 0.6$	
BC	$a_{1,i} = 1.5$, $a_{2,i} = 2$	

The simulations account for a 30% variation in the inertia moments to represent model uncertainty. Starting at $t = 15$ s for forces and $t = 10$ s for moments, the aerodynamic disturbances acting on the system are given by:

$$\begin{aligned} \mathbf{d}_\xi(t) &= \left[\cos(4\pi t + 2\pi),\ \sin(4\pi t + 2\pi),\ \sin(4\pi t)\right]^\top \text{N} \\ \mathbf{d}_\eta(t) &= \left[0.3\sin(\tfrac{\pi t}{3}),\ 0.3\cos(\tfrac{\pi t}{3}),\ 0.5\sin(\tfrac{\pi t}{3} + \tfrac{\pi}{3})\right]^\top \text{N.m} \end{aligned} \tag{4.1}$$

4.1. Path following simulation

Figures 2–4 present the simulation results obtained to evaluate the overall control performance of the proposed framework. Figure 2 depicts the translational motion tracking performance of the quadrotor UAVs along the three Cartesian axes x, y, and z. The results demonstrate that the actual positions closely follow the prescribed stepwise desired trajectories, achieving fast transient responses and stable convergence. A small overshoot and nearly zero steady-state error are observed across all three axes, highlighting the controller's ability to ensure accurate and robust position tracking despite the presence of external disturbances and model uncertainties. Figure 3 presents the rotational tracking results of the quadrotor in terms of the three Euler angles, namely, roll (ϕ), pitch (θ), and yaw (ψ). It is observed that the yaw angle successfully follows the desired step reference signals with rapid convergence, high accuracy, and very small overshoot. Similarly, the roll and pitch angles generated by the inner loop controller accurately track their respective reference trajectories smoothly and stably, confirming the robustness and effectiveness of the proposed controller in handling rotational dynamics. Figure 4 shows the control inputs Ω_1, Ω_2, Ω_3, and Ω_4, corresponding to the angular velocities of the four rotors. The signals initiate near a nominal hovering value, indicating initial steady hover conditions. Around $t \approx 40$ s, moderate oscillations appear as the controller compensates for time-varying attitude references. Brief transient peaks at $t \approx 15$ s and $t \approx 80$ s are associated with abrupt reference changes induced by external disturbances. Overall, the control inputs remain well bounded, confirming smooth actuator behavior and stable closed-loop attitude tracking.

4.2. Comparative study

To assess the effectiveness of the proposed approach, four control schemes are examined: the proposed adaptive fixed-time disturbance observer-based cascade filtered fixed-time backstepping controller (AFxTDOBC), the extended state observer-based controller (ESOBC) [28], the finite-time backstepping controller (FTBC) [29], and the backstepping controller (BC) [30]. The comparative results are illustrated in Figures 5–8. Figure 5 compares the translational position tracking performance of the quadrotor along the x, y, and z axes for the four considered control strategies. The proposed AFxTDOBC achieves the fastest convergence and highest steady-state accuracy across all three axes, owing to its integrated disturbance observer, which ensures strong robustness against external perturbations. The ESOBC also performs satisfactorily but exhibits slightly slower settling time and larger steady-state errors, particularly along the x-axis. The FTBC shows moderate performance with noticeable convergence delays and tracking errors, especially along the y and z axes. The BC displays the slowest convergence, largest steady-state errors, and weakest robustness among all the evaluated controllers, particularly along the z-axis, confirming the limitations associated with the absence of disturbance compensation mechanisms. Figure 6 presents the rotational tracking performance of the quadrotor expressed in terms of the three Euler angles, namely, yaw (ψ), roll (ϕ), and pitch (θ), for the four considered control schemes. Among all evaluated controllers, the AFxTDOBC maintains the best tracking accuracy with minimal phase lag, and the embedded disturbance observer allows it to effectively attenuate rapid oscillations and sudden reference changes. The ESOBC demonstrates comparable performance but exhibits slightly greater deviation from the reference signals, particularly during yaw step changes and oscillatory roll and pitch transients. The FTBC exhibits moderate tracking accuracy, however, its performance degrades noticeably when the reference signals undergo rapid

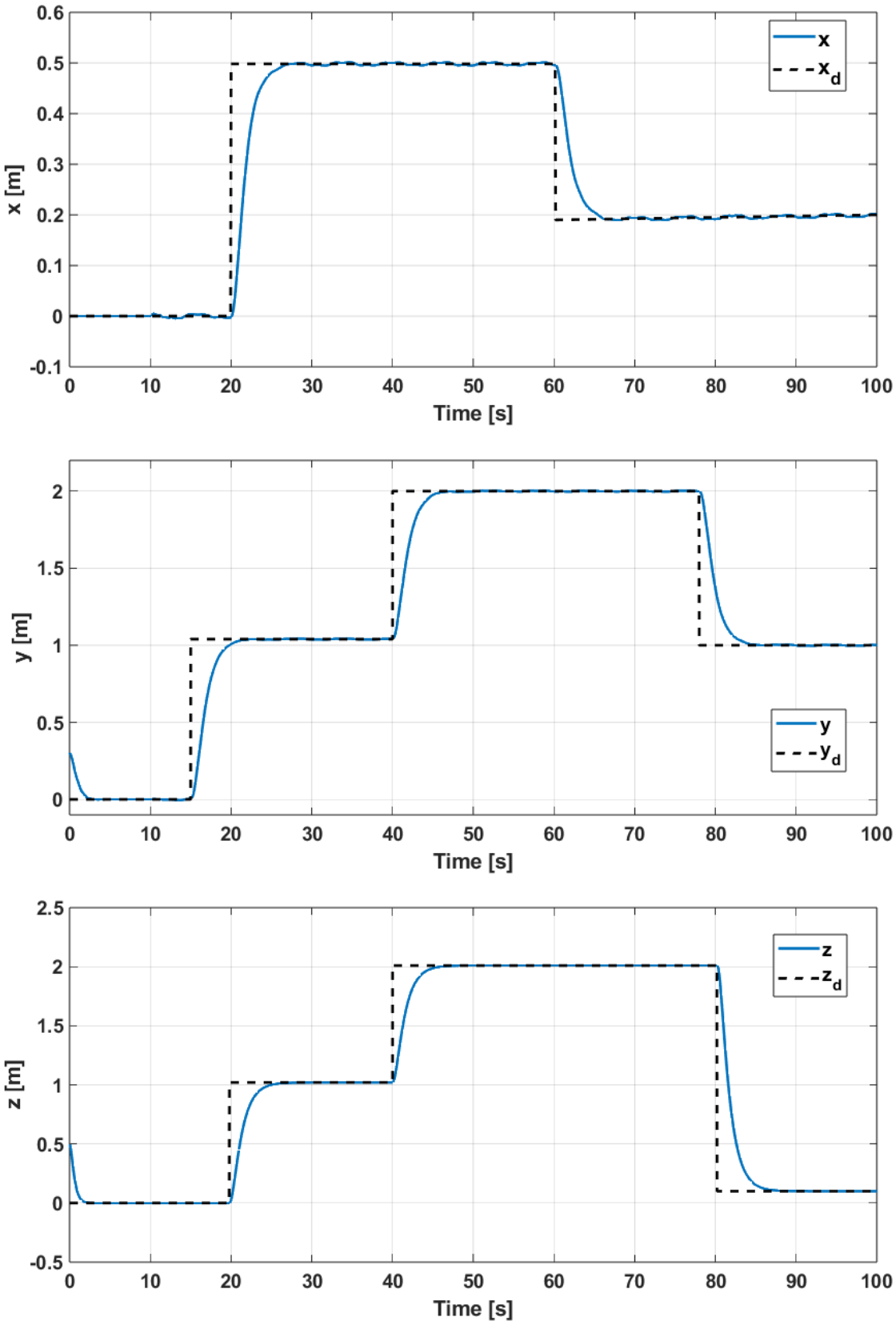

Figure 2. Translational trajectories of the QUAV.

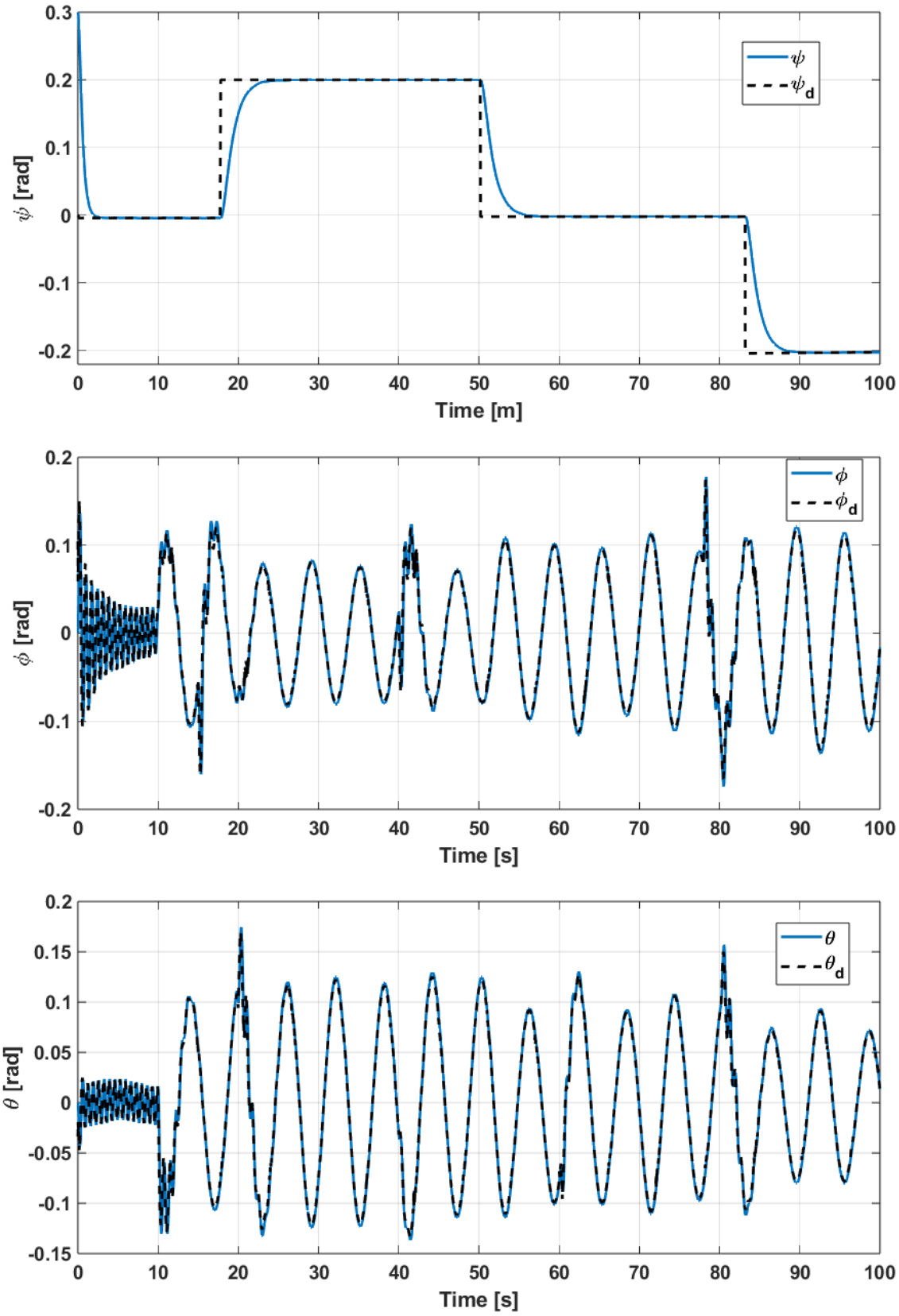

Figure 3. Rotational trajectories of the QUAV.

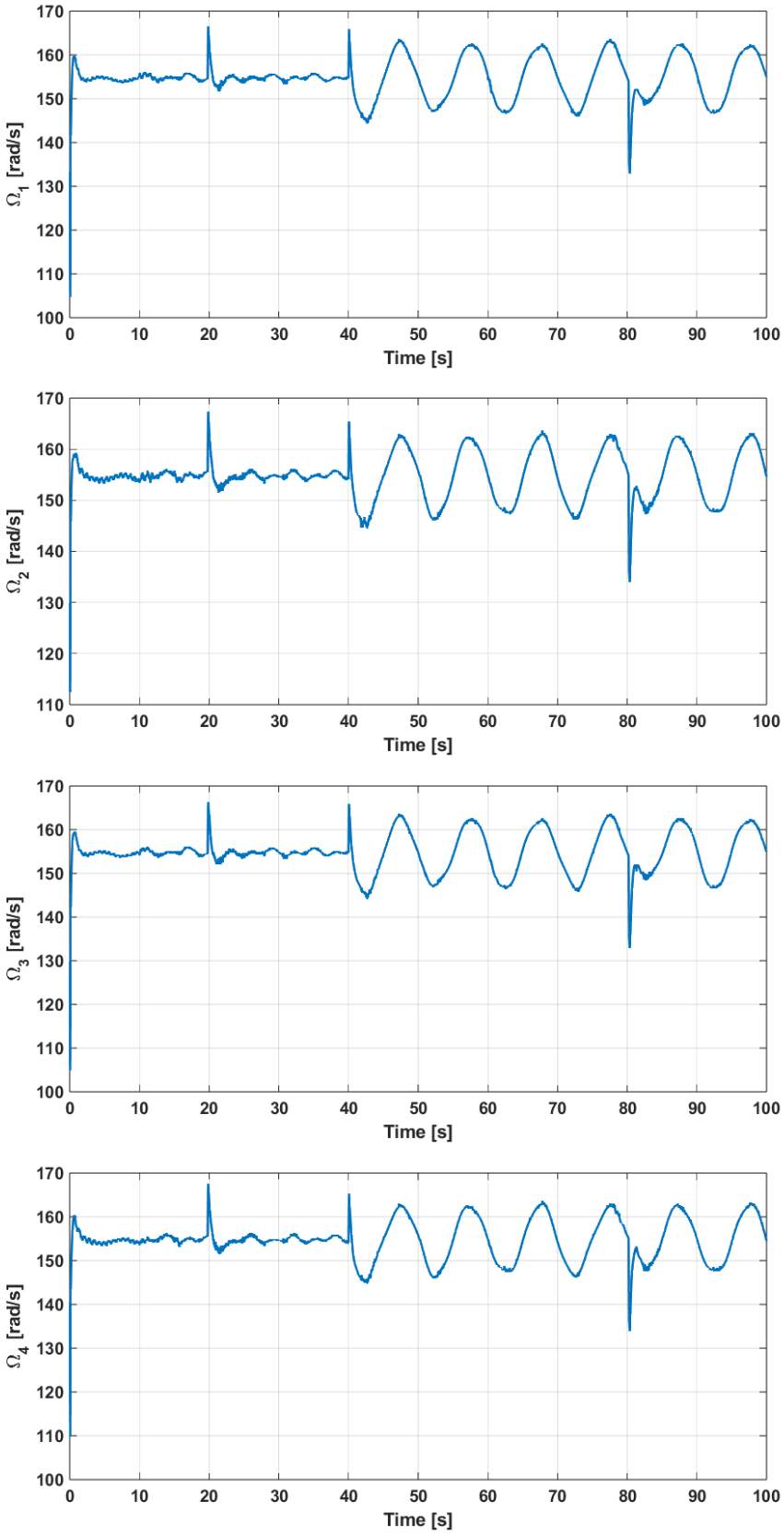

Figure 4. Control signals.

variations, especially in the roll and pitch channels. BC yields the weakest tracking performance overall, suffering from the largest phase lag and the most significant deviation from the desired trajectories, underscoring the impact of the absence of fixed-time convergence and disturbance rejection properties.

Figures 7 and 8 depict the translational and rotational tracking errors obtained for all four controllers. The proposed AFxTDOBC achieves the smallest errors and fastest convergence in both translational and rotational dynamics. The ESOBC performs comparably but with slightly larger residual errors. The FTBC and BC exhibit the largest error peaks, especially during abrupt reference changes, further highlighting the advantage of the proposed AFxTDOBC's disturbance observer in maintaining precise and robust tracking throughout all operating conditions.

5. Conclusions

This paper presents a novel robust control framework based on fixed-time filtered backstepping for autonomous trajectory tracking of quadrotor UAV subject to model uncertainties and external disturbances. In contrast to conventional asymptotic or finite-time approaches, the proposed strategy guarantees convergence within a settling time that is explicitly independent of initial conditions, thereby providing predictable transient performance and enhanced reliability for mission-critical operations. A cascade fixed-time backstepping architecture is systematically constructed by embedding a virtual control law with strict fixed-time convergence properties into a command filtering mechanism. This formulation inherently resolves the explosion-of-complexity problem associated with classical backstepping, yielding smoother control signals and significantly reduced computational burden without compromising stability guarantees. To enhance robustness against lumped uncertainties and time-varying disturbances, an adaptive fixed-time disturbance observer is incorporated into the control architecture. The adaptive term of the observer dynamically adjusts its parameters based on the measured system errors, allowing the observer to track unknown external disturbances without prior knowledge of their magnitude or structure. The observer provides an accurate estimation of unknown perturbations within a guaranteed fixed-time interval, enabling precise feedforward compensation and improved closed-loop performance. The stability of the overall closed-loop system, including the boundedness of all tracking errors, is rigorously established via Lyapunov-based analysis. Extensive numerical simulations under multiple operating scenarios, including parametric variations and external disturbance injections, validate the theoretical results. Comparative evaluations against existing controllers consistently demonstrate superior tracking accuracy, faster transient response, reduced steady-state error, and stronger disturbance rejection, confirming the practical viability of the proposed framework for advanced quadrotor applications. Nevertheless, the proposed control approach has some limitations. It demands substantial computational resources, which may restrict real-time implementation on low-power embedded systems. While simulations demonstrate strong performance, real-world factors such as sensor noise, actuator delays, and aerodynamic effects can introduce additional challenges in practical UAV deployment. Furthermore, extending the framework to larger or more complex UAV systems with additional degrees of freedom may require extra hierarchical layers and careful design to maintain stability guarantees.

As future work, the proposed framework can be extended to more complex underactuated aerial systems, such as aerial manipulators with higher degrees of freedom. Further research may focus

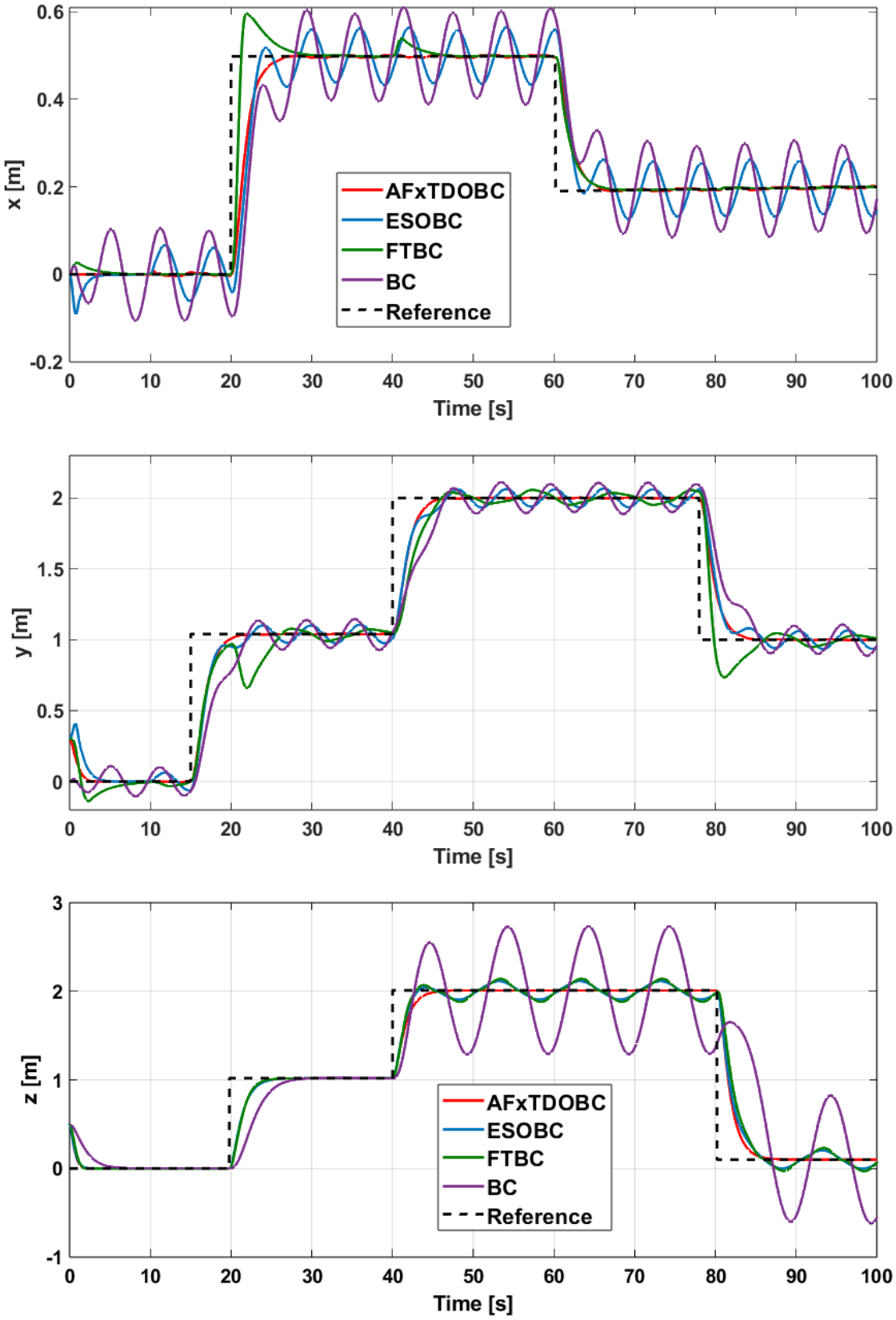

Figure 5. Translational trajectories of the QUAV with different controllers.

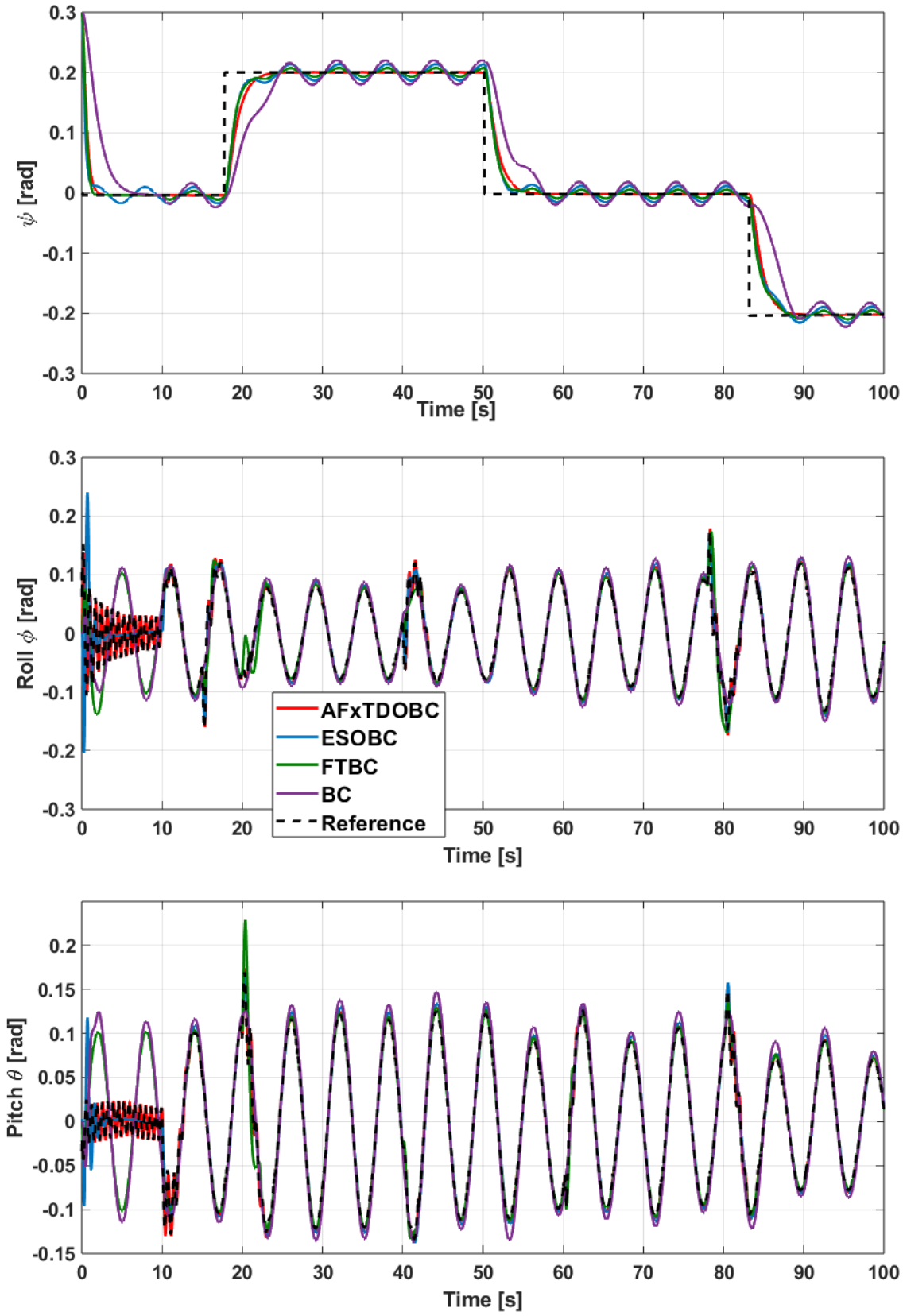

Figure 6. Rotational trajectories of the QUAV with different controllers.

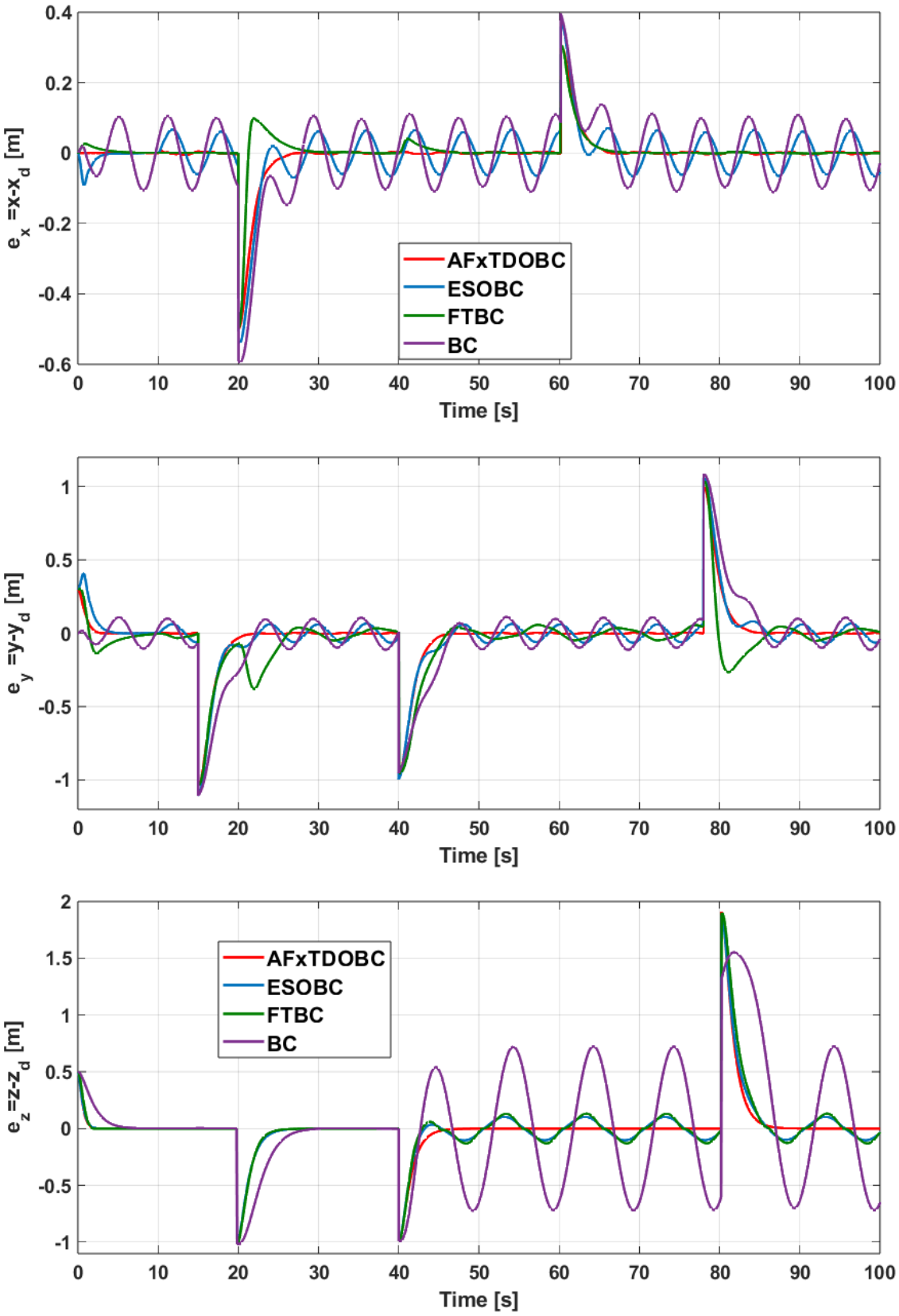

Figure 7. Translational tracking errors of the QUAV with different controllers.

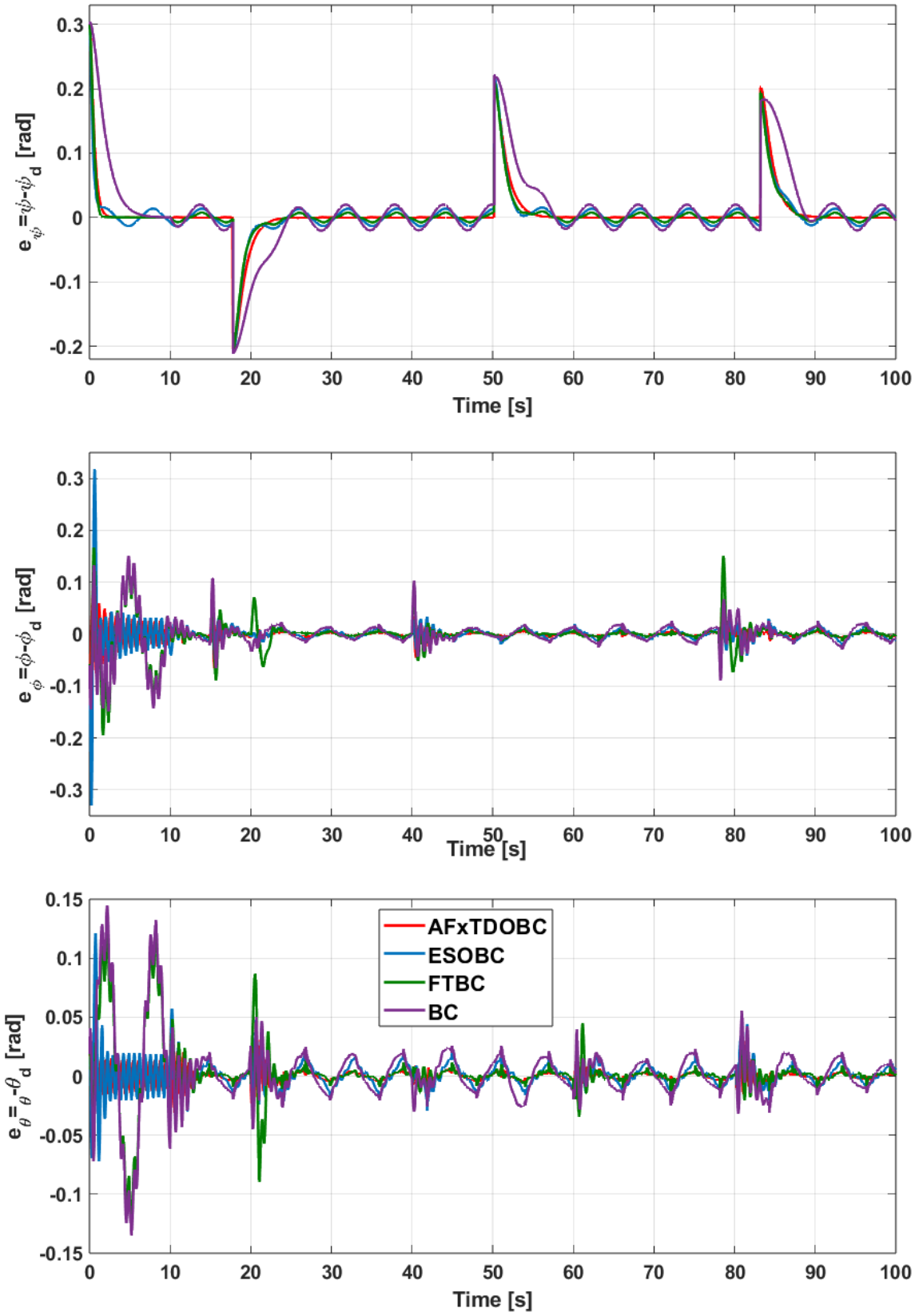

Figure 8. Rotational tracking errors of the QUAV with different controllers.

on adaptive predefined-time control strategies for systems with completely unknown dynamics, the integration of machine learning techniques to enhance performance in highly uncertain environments, and the development of novel predefined synergetic control approaches. Moreover, experimental validation and real-world implementation on full-scale autonomous aerial platforms, such as the Quanser platform, remain important directions for future investigation.

Author contributions

Mohammed Rida Mokhtari: conceptualization, methodology, software, formal analysis, investigation, writing and editing, visualization, supervision; Abdelkader Ghezouani and Bensalah Choukri: investigation, supervision; Amal Choukchou Braham: supervision, project administration; Hicham Megnafi: supervision.

Use of Generative-AI tools declaration

The authors declare they have not used Artificial Intelligence (AI) tools in the creation of this article.

Conflict of interest

All authors declare no conflicts of interest in this paper.

References

1. Obaid L, Hamad K, Al-Ruzouq R, Abu Dabous S, Ismail K, Alotaibi E (2025) State-of-the-art review of unmanned aerial vehicles (UAVs) and artificial intelligence (AI) for traffic and safety analyses: Recent progress. applications, challenges, and opportunities. *IEEE Lat Am T* 13: 101591. https://doi.org/10.1109/TLA.2016.7785923
2. Nahata D, Othman K (2023) Exploring the challenges and opportunities of image processing and sensor fusion in autonomous vehicles: A comprehensive review. *AIMS Electronics and Electrical Engineering* 7: 271–321. https://doi.org/10.3934/electreng.2023016
3. Albarghot M, Iqbal MT, Pope K, Rolland L (2020) Dynamic modeling and simulation of the MUN Explorer autonomous underwater vehicle with a fuel cell system. *AIMS Electronics and Electrical Engineering* 4: 114–131. https://doi.org/10.3934/ElectrEng.2020.1.114
4. Torres FJ, Guerrero GV, García CD, Gómez JF, Adam M, Escobar RF (2016) Master-Slave Synchronization of Robot Manipulators Driven by Induction Motors. *IEEE Lat Am T* 42: 3986–3991. https://doi.org/10.1109/TLA.2016.7785923
5. Bensalah C, Mokhtari MR, Braham AC (2026) A new approach for solving the aerial manipulator inverse kinematics. *Journal of the Franklin Institute* 362: 107912. https://doi.org/10.1016/j.jfranklin.2025.107912
6. Mokhtari MR, Braham AC (2016) Disturbance Observer-based Approximate Linearization Control of Gun Launched MAV. *Electrotehnica, Electronica, Automatica* 64: 131.

7. Zeng Y, Yang G, Wang Z (2025) Active disturbance rejection geometric control of quadrotor UAV on SO(3). *Journal of the Franklin Institute* 362: 107–744. https://doi.org/10.1016/j.jfranklin.2025.107744
8. Mokhtari MR, Braham AC, Cherki B (2023) Finite-time extended state observer based sliding mode control for a VTOL multi-rotors UAV. *IEEE International Workshop on Mechatronic Systems Supervision (IW_MSS)*, 1–6. https://doi.org/10.1109/IW_MSS59200.2023.10369931
9. Wan M, Chen M, Yong K (2022) Adaptive tracking control for an unmanned autonomous helicopter using neural network and disturbance observer. *Neurocomputing* 468: 296–305. https://doi.org/10.1016/j.neucom.2021.09.060
10. Liu W, Cheng X, Zhang J (2023) Command filter-based adaptive fuzzy integral backstepping control for quadrotor UAV with input saturation. *Journal of the Franklin Institute* 360: 484–507. https://doi.org/10.1016/j.jfranklin.2022.10.042
11. Chávez-Vázquez S, Gómez-Aguilar JF, Lavín-Delgado JE, Escobar-Jiménez RF, Olivares-Peregrino VH (2022) Applications of Fractional Operators in Robotics: A Review. *J Intell Robot Syst* 104: 63. https://doi.org/10.1007/s10846-022-01597-1
12. Chen L, Jia Y, Sun S, Lv Z, Wu Y (2025) Immersion and invariance adaptive controller and mixer for coaxial tilt-rotor UAV. *ISA Transactions* 166: 353–363. https://doi.org/10.1016/j.isatra.2025.07.015
13. Zeghlache S, Rahali H, Djerioui A, Benyettou L, Benkhoris M (2024) Robust adaptive backstepping neural networks fault tolerant control for mobile manipulator UAV with multiple uncertainties. *Math Comput Simulat* 218: 556–585. https://doi.org/10.1016/j.matcom.2023.11.037
14. Van An V, Mien TL, Van Binh N (2026) A comprehensive survey of UAV control algorithms: Integrating classical methods with artificial intelligence for enhanced trajectory tracking. *AIMS Electronics and Electrical Engineering* 10: 26–53. https://doi.org/10.3934/electreng.2026002
15. Chávez-Vázquez S, Gómez-Aguilar JF, Lavín-Delgado JE, Escobar-Jiménez RF, Olivares-Peregrino VH (2022) Intelligent Neural Integral Sliding-mode Controller for a space robotic manipulator mounted on a free-floating satellite. *Adv Space Res* 71: 3734–3747. https://doi.org/10.1016/j.asr.2022.08.053
16. Qin H, Si J, Wang N, Gao L (2023) Fast fixed-time nonsingular terminal sliding-mode formation control for autonomous underwater vehicles based on a disturbance observer. *Ocean Eng* 270: 113–423. https://doi.org/10.1016/j.oceaneng.2022.113423
17. Li Y, Liu K, Wen CY, Liu X, Zhang W, Zheng Y (2025) Fast fixed-time incremental backstepping fault-tolerant control for aircraft with asymmetric wing damage. *Aerosp Sci Technol* 164: 110–405. https://doi.org/10.1016/j.ast.2025.110405
18. Jiao D, Wang Y, Chen Y, Lu W, Zou AM, Yang X (2025) Finite-time attitude control for fixed-wing UAVs with full-state constraints and input saturation. *Journal of the Franklin Institute* 362: 107–522. https://doi.org/10.1016/j.jfranklin.2025.107522
19. Najafi A, Mobayen S, Jalilvand A (2025) Fixed-time anti-saturation and fault-tolerant control for quadrotor UAVs using event-trigger adaptive barrier sliding mode control. *ISA Transactions* 167: 44–64. https://doi.org/10.1016/j.isatra.2025.08.030

20. Yu B, Du H, Zhu W, Cong Y (2025) A vector-type finite-time trajectory tracking controller for quadrotor UAVs with safety constraints. *Aerosp Sci Technol* 163: 110–254. https://doi.org/10.1016/j.ast.2025.110254
21. Guan Z, Liu H, Zheng Z, Lungu M, Ma Y (2021) Fixed-time control for automatic carrier landing with disturbance. *Aerosp Sci Technol* 108: 106–403. https://doi.org/10.1016/j.ast.2020.106403
22. Polyakov A (2012) Nonlinear feedback design for fixed-time stabilization of linear control systems. *IEEE T Automat Contr* 57: 2106–2110. https://doi.org/10.1109/TAC.2011.2179869
23. Tran XT, Oh H (2021) A modified generic second-order algorithm with fixed-time stability. *ISA Transactions* 109: 72–80. https://doi.org/10.1016/j.isatra.2020.10.021
24. Liu Y, An S, Wang L, Fan Z (2025) Predefined time backstepping control with an adaptive predefined time disturbance observer for underactuated AUV under unknown external disturbance. *Ocean Eng* 340: 122382. https://doi.org/10.1016/j.oceaneng.2025.122382
25. Xie S, Chen Q (2021) Adaptive nonsingular predefined-time control for attitude stabilization of rigid spacecrafts. *IEEE T Circuits-II* 69: 189–193. https://doi.org/10.1109/TCSII.2021.3078708
26. Mokhtari MR, Bensalah C, Laribi N, Braham AC (2026) Fixed-time observer-based filtered hierarchical control for a gun-launched coaxial rotor vehicle. *Proceedings of the Institution of Mechanical Engineers, Part I: Journal of Systems and Control Engineering*, 09596518251399967. https://doi.org/10.1177/09596518251399967
27. López-Sánchez I, Pérez-Alcocer R, Moreno-Valenzuela J (2023) Trajectory tracking double two-loop adaptive neural network control for a quadrotor. *Journal of the Franklin Institute* 360: 3770–3799. https://doi.org/10.1016/j.jfranklin.2023.01.029
28. Sinan S, Ghommam J, Saad M, Fareh R, Bettayeb M (2025) Cascaded extended-state-observer-based synergetic control for quadcopter translational dynamics. *J Field Robot* 42: 3153–3171. https://doi.org/10.1002/rob.22566
29. Patel N, Paul CK, Kar IN, Mukherjee S (2024) Finite time adaptive backstepping control approach for quadrotors. *IFAC-PapersOnLine* 57: 89–94. https://doi.org/10.1016/j.ifacol.2024.05.016
30. Mokhtari MR, Nesserine L (2024) Research on a combinatorial control Method for small aerial vehicles based on disturbance compensation techniques. *IEEE International Multi-Conference on Smart Systems & Green Process (IMC-SSGP)*, 1–6. https://doi.org/10.1109/IMC-SSGP63352.2024.10919745

AIMS Press